Analysis and Computation for Coupling

Bose-Einstein Condensates in Optical Resonators

Xu Wei Biao

NATIONAL UNIVERSITY OF SINGAPORE

2010

Analysis and Computation for Coupling

Bose-Einstein Condensates in Optical Resonators

Xu Wei Biao

(B.Sc. Sun Yat-Sen University of China)

A THESIS SUBMITTED FOR THE DEGREE OF

MASTER OF SCIENCE

DEPARTMENT OF MATHEMATICS

NATIONAL UNIVERSITY OF SINGAPORE

2010

Acknowledgements

First of all, I would like to sincerely express my thanks to my supervisor, Prof Bao Weizhu for his thoughtful kindness and priceless guidance. He gave me great encouragement and help when I was in a maze and patiently led me to the right way in both research and life.

Furthermore, many thanks go to my senior, Dr Wang Hanquan for nurturing my mathematical maturity. He shared his valuable experience in research work and offered me great help on my thesis.

I would also like to thank my family and friends, for their unconditional love and support. Special thanks go to Zhou Fan, Sit Wing Yee, Goh Siong Thye, Dong Xuan Chun, Wong Weipin, Tang Qinglin and Zhang Yong. It is my honor to have these friends.

Last not the least, I am grateful for the financial support from the National University of Singapore and Ministry of Education of Singapore. Without the scholarship provided for me, I would not be able to pursue my dream in study.

Xu Wei Biao

Aug 2010

Contents

Summary

Since 1995, Bose-Einstein condensates (BEC) of alkali atoms have been produced and studied extensively in experiments. One central goal of experiments has been formation of Bose-Einstein condensates with a number of atoms as large as possible. Based on mean field theory, Jaksch et al. recently proposed a mathematical model—Gross-Pitaevskii equations coupled with an integral and ordinary differential equation in order to study the possibility of how to unite two BEC in optical resonators. However, the authors investigated this possibility through two-mode analysis of the mathematical model. In this thesis, we propose efficient numerical methods—Sine pseudospectral methods to solve the mathematical model and perform direct numerical simulations on studying such possibility.

We first investigate the ground state solutions of two coupling BEC, which describe the equilibrium state of the coupling BEC in optical resonators at extremely low temperature. We compute the ground state solutions by proposing a normalized gradient flow discretized with backward Euler Sine pseudospectral approach. We use our numerical one-dimensional and two-dimensional solutions to study which factors may be useful for uniting BEC in optical resonators at equilibrium.

We next study the dynamics of two coupling BEC in optical resonators by designing new efficient numerical methods—time-splitting Sine pseudospectral methods for the Gross-Pitaevskii equations coupled with an integral and ordinary differential equation. Though there is an extra ordinary differential equation with integral term in the mathematical model for the dynamics of coupling BEC in optical resonators, which may bring us some numerical difficulties, we successfully adapt the usual time-splitting methods to deal with them. The proposed numerical methods keep the dynamical properties of the mathematical model very well in the discretized level and have spectral accuracy in space. The numerical results obtained by these efficient numerical methods are used to analyze the possible way of dynamically uniting BEC in optical resonators.

List of Tables

List of Figures

Chapter 1

Introduction

The Bose-Einstein condensate (BEC) is a state of interacting bosons, which is cooled to the temperature close to absolute zero ($-273.15°$C). Under such strict condition, a large part of bosons will condense into the lowest energy state, which is the so called quantum mechanical ground state (cf. Figure 1.1). In this chapter, we first introduce brief history of the development of BEC, and then we review some theoretical studies of single-component BEC. Finally we introduce recent development of BEC and our problem to be investigated in the thesis.
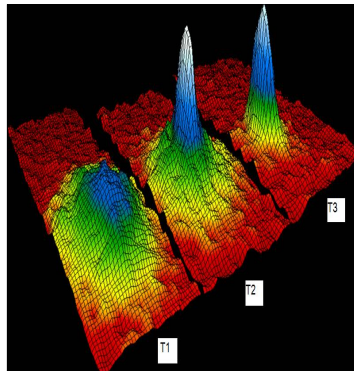
Figure 1.1: Velocity-distribution data of rubidium-87. From temperature T1 to T3, the temperature becomes lower and lower. T1 is the temperature before the appearance of a BEC; at T2, the condensate appears; and at T3, nearly pure condensate is formed. (taken from Wikipedia).

1.1 Development of BEC

Based on a statistical description of photons done by an Indian physicist Satyendra Nath Bose (1924) [3], a phenomenon was predicted by Einstein (1925) [20] that a BEC could occur in a gas of noninteracting atoms below some critical temperature in the form of phase transition.

In 1938, Pyotr Kapitsa, John Allen and Don Misener discovered superfluid from helium-4 below temperature $2.17K$, whose superfluidity was due to partial BEC of the liquid. Later F. London showed that the superfluidity could be a manifestation of the BEC. However, because of the limitation of technique, only a small fraction of condensate was found in the experiments on superfluid till 1955. While in the 1970s, the BEC was almost achieved when studies on dilute atomic gases were set up, but it was still not pure [47].

With the development of laser and magnetic evaporative cooling techniques, the first pure BEC, in vapors of rubidium-87 (cf. Figure 1.1) and sodium-23, was observed separately by Eric Cornell, Carl Wieman at JILA and by Ketterle at MIT on 1995. Later, it was achieved on many other atoms such as helium-4, rubidium-85 and spin-polarized hydrogen.

New developments in dilute atomic gas unveiled remarkable properties of the BEC [67]. The most remarkable one is the so-called wave-like behavior of matter, which is shown on a macroscopic scale due to condensation of a large number of identical atoms into the same quantum state. If the interactions between particles are weak in a dilute atomic gas, the wave-like condensate can be summed up and described by a single particle to show an average effect. This gives rise to the macroscopic wave function $\psi(\mathbf{x}, t)$ whose evolution is governed by a self-consistent, mean field nonlinear Schrödinger equation known as the Gross-Pitaevskii equation (GPE) [23, 46]

$$
\begin{aligned}
i\hbar \frac{\partial \psi(\mathbf{x}, t)}{\partial t} &= \frac{\delta E(\psi)}{\delta \bar{\psi}} \\
&= -\frac{\hbar^2}{2m} \nabla^2 \psi(\mathbf{x}, t) + V(\mathbf{x})\psi(\mathbf{x}, t) + U|\psi(\mathbf{x}, t)|^2 \psi(\mathbf{x}, t), \quad (1.1)
\end{aligned}
$$

where $\mathbf{x} = (x, y, z)^T$ is the spatial coordinate vector; $\hbar$ is the Planck constant; $\bar{\psi}$ is

the conjugate of ψ; m is the atomic mass; $V(\mathbf{x})$ is an external trapping potential; $U = \frac{4\pi\hbar^2 a_s}{m}$ describes the interactions between atoms in the condensate; a_s is atomic scattering length. The energy of the system $E(\psi)$ can be defined as

$$E(\psi) = \int_{\mathbb{R}^3} \left[\frac{\hbar^2}{2m} |\nabla\psi(\mathbf{x},t)|^2 + V(\mathbf{x})|\psi(\mathbf{x},t)|^2 + \frac{U}{2}|\psi(\mathbf{x},t)|^4 \right] d\mathbf{x}. \qquad (1.2)$$

1.2 Numerical methods on single BEC

Numerical studies on single BEC models mostly concentrate on finding ground states and simulating dynamical process via GPE (1.1). These studies provide powerful tools for subsequent researches on BEC. In this section, we review the main numerical methods for solving the GPE (1.1) in the study of single BEC.

To compute the ground state, there are two kinds of schemes: (i) finite difference scheme, and (ii) pseudospectral scheme. In the former, Edwards and Burnetts [21] introduced a Runge-Kutta method to solve GPE for 1D ground state and 3D ground state with spherical symmetry; Bao and Du [5] proposed a backward Euler finite difference method to discretize continuous normalized gradient flow with diminishing energy; and Ruprecht et al. [50] presented a Crank-Nicolson finite difference method. For the latter scheme, Bao et al. [7, 9] introduced a sine pseudospectral method to discretize continuous normalized gradient flow for computing ground state. Each of these two schemes has its advantages and disadvantages. The finite difference scheme is only of second order spatial accuracy although it is implicit and unconditionally stable, while pseudospectral scheme is of spectral accuracy in space, but it is conditionally stable [67].

To study the dynamics of the BEC, we can classify the methods into two groups: (i) the finite difference methods which include Crank-Nicolson finite difference method [50], alternating direction implicit method [57] and explicit finite difference method [17]; (ii) the pseudospectral methods which include the TSSP [6, 7] and Runge-Kutta pseudo-spectral method [2, 36]. These two kinds of methods are vastly applied in physical and mathematical literatures. In numerical computation, we favor pseudospectral methods rather than the finite difference methods since pseudospectral methods have high-order accuracy.

1.3 Contemporary studies in BEC

With the development of technologies in experiments, various aspects of BEC have been investigated. Quantized vortices in a BEC are recently obtained in experiments by several groups, e.g. the JILA [35], ENS [34, 49] and MIT [48]; Another important recent development in BEC was the study of spin-1 and spin-2 condensates. The spin-1 BEC was realized in experiments by using both sodium-23 and rubidium-87. BEC with multiple species have also been achieved in experiments [25, 24, 30, 37, 52]. In addition, the first experiment of two-component BEC was performed in JILA [37], and extensive studies on multiple-component BEC have been carried out. The experimental progress in BEC has greatly propelled the theoretical studies on BEC.

Subsequent numerical simulations and theoretical studies on BEC illustrated existent experimental results in recent years. For a non-rotating BEC, Lundh et. al [33] investigated free expansion of vortex state, Bao and Du [5] computed central vortex states; For a rotating BEC, several groups e.g. Bao et. al [6, 11], Jackson et. al [28, 29], and Caradoc-Davis et. al [15, 16], simulated generation of vortices from the ground state and studied dynamics of vortices, Svidzinsky and Fetter [55] investigated dynamics of a vortex line which depends on its curvature, Modugno et. al [38] and Aftalion et. al [1] presented bent vortices like S-shaped and U-shaped vortex, and compared with experimental results [49]; A spin-F BEC was described by the coupled GPEs [47, 46, 23], and dynamical laws of the coupled GPEs for spin-1 BEC were proposed by Bao and Zhang [12], while Wang [61] presented dynamics of spinor F=1 BEC. Moreover, Bao [4] provided a mathematical justification by computing ground states and dynamics of multi-component BEC, Lieb and Solovej [31] investigated the ground state energy of the two-component charged Bose gas, Wang [62] presented numerical simulations on stationary states for rotating two-component Bose-Einstein condensates while Bao et al. [13] computed the dynamics.

Although tremendous simulation results have been carried out, there are still lots of challenging theoretical problems for multi-component BEC. One recent goal of physical experiments is to form BEC with the numbers of atoms as large as possible. Therefore, it is particularly interesting to realize the goal by forming a large single BEC via uniting

two or more independent condensates.

1.4   The problem

Recently Jaksh et al. proposed that two initially independent BEC could be united to one large BEC by putting them into a ring cavity and coupling them with an internal Josphson junction [27, 64]. The experiment setup of the proposal are (cf. Figure 1.2(a)) : Two initially independent condensates 1 and 2 trapped in a ring cavity are coupled with two lasers Ω and Ω_1 as well as the cavity mode. The Level structures of the experiments are (cf. Figure 1.2(b)): Atoms are transferred by Raman laser Ω from level $|1>$ to level $|2>$. Another transition between particles in level $|1>$ and an auxiliary level $|3>$ is drived by laser Ω_1. The cavity couples the levels $|3>$ and $|2>$ with the coupling strength g_c. In this experimental setup, the two condensates are trapped in many optical resonators [64].
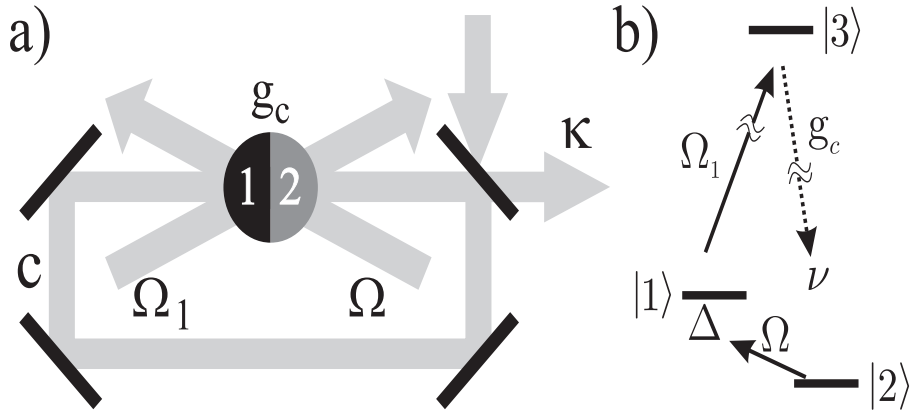
Figure 1.2: (a) Experiment setup, (b) Level structure. (taken from [27]).

According to the mean field theory, at extremely low temperature, the mathematical model for describing the above-mentioned coupling BEC in optical resonators is the

following coupled equations [25, 27, 64]

$$i\hbar\frac{\partial\psi(\mathbf{x},t)}{\partial t} = -\frac{\hbar^2}{2m}\nabla^2\psi(\mathbf{x},t) + V_1(\mathbf{x})\psi(\mathbf{x},t) + \left[u_{11}|\psi(\mathbf{x},t)|^2 + u_{12}|\phi(\mathbf{x},t)|^2\right]\psi(\mathbf{x},t)$$

$$+\hbar(\hat{g}C(t) + \frac{\hat{\Omega}}{2})\phi(\mathbf{x},t) + \hbar\hat{\delta}_1\psi(\mathbf{x},t), \tag{1.3}$$

$$i\hbar\frac{\partial\phi(\mathbf{x},t)}{\partial t} = -\frac{\hbar^2}{2m}\nabla^2\phi(\mathbf{x},t) + V_2(\mathbf{x})\phi(\mathbf{x},t) + \left[u_{21}|\phi(\mathbf{x},t)|^2 + u_{22}|\psi(\mathbf{x},t)|^2\right]\phi(\mathbf{x},t)$$

$$+\hbar(\hat{g}\bar{C}(t) + \frac{\hat{\Omega}}{2})\psi(\mathbf{x},t) + \hbar\hat{\delta}_2\phi(\mathbf{x},t), \tag{1.4}$$

$$i\hbar\frac{\partial C(t)}{\partial t} = \hbar\int_{\mathbb{R}^3}\hat{g}\bar{\phi}(\mathbf{x},t)\psi(\mathbf{x},t)d\mathbf{x} + \hbar\hat{v}C(t), \quad \mathbf{x}\in\mathbb{R}^3, \ t>0. \tag{1.5}$$

Here, $\psi(\mathbf{x},t)$, $\phi(\mathbf{x},t)$ denote two wave functions of two coupling condensates, $|C(t)|^2$ represents number of photons in the cavity at time t, $u_{jk} = \frac{4\hbar^2\pi a_{jk}}{m}$ $(j,k = 1,2)$ are the interactions, a_{jk} is the s-wave scatting length for interspecies, $\hat{\delta}_k$, $k = 1,2$, is the effective detuning strength of condensates and $\hat{v}$ is the effective detuning strength of the ring cavity, $\hat{\Omega}$ is frequency, and $\hat{g}$ is the coupling strength of the ring cavity mode. $V_k(\mathbf{x})$, $k = 1,2$, are the external trapping potentials and they take the form

$$V_k(\mathbf{x}) = \frac{m}{2}\left[\omega_{x,k}^2 x^2 + \omega_{y,k}^2 y^2 + \omega_{z,k}^2 z^2\right], \ k = 1,2,$$

if they are harmonic. (1.5) is also called mode equation which describes the property of optical cavity.

In [27], the authors investigate how to unite two independent condensates into a single one through two-mode analysis of the coupled equations (1.3)-(1.5) and Monte-carlo simulations. In this thesis, based on direct numerical solutions of the coupled equations (1.3)-(1.5), we study ground state and dynamics of coupling BEC in optical resonators, which may shed light on how two independent condensates could be united to one BEC.

1.5 Overview of this work

The structure of this thesis is as follows.

In Chapter 2, we simplify the model into a dimensionless form by rescaling the parameters and then we reduce the three dimensional model into lower dimensional

models. Last we define the energy for the whole system and prove the conservation properties of mass and energy.

In Chapter 3, we first define the ground state for our model. We then compute the ground state by constructing a normalized gradient flow discretized with backward Euler Sine pseudospectral approach. Lastly we investigate the ground state of coupling BEC in optical resonators for 1D and 2D cases.

In Chapter 4, we start off by investigating dynamical laws and then we solve the mathematical model by using time-splitting Sine pseudospectral methods for the coupled equations. Though there is an ODE with integral term in the mathematical model for the dynamics of coupling BEC in optical resonators, which may bring some difficulties in practical computation, we successfully adjust the usual time-splitting methods to solve the model. Next, we test the convergence of our schemes and observe various dynamics of coupling BEC in optical resonators through intensive numerical simulations.

In Chapter 5, we draw some conclusions of this work and inspire some ideas on future directions.

Chapter 2

Coupled BEC in optical resonators

In this chapter, we first reformulate the coupled equations (1.3)-(1.5) into a dimensionless formulation. Furthermore, for simplification of our study, we reduce the dimensionless three-dimensional coupled equations into two-dimensional coupled equations and one-dimensional coupled equations, respectively. Last, we investigate some conservation properties of coupled equations in optical resonators.

2.1 Dimensionless formulation

To derive the dimensionless formulation for equations (1.3)-(1.5), we introduce $a_0 = \sqrt{\frac{\hbar}{m\omega_{x,1}}}$, $\tilde{\mathbf{x}} = \frac{\mathbf{x}}{a_0}$, $\tilde{t} = \omega_{x,1}t$, $\tilde{\psi}(\tilde{\mathbf{x}}, \tilde{t}) = \frac{a_0^{\frac{3}{2}}\psi(\mathbf{x},t)}{\sqrt{N}}$, $\tilde{\phi}(\tilde{\mathbf{x}}, \tilde{t}) = \frac{a_0^{\frac{3}{2}}\phi(\mathbf{x},t)}{\sqrt{N}}$, $\tilde{C} = \frac{C}{\sqrt{N}}$, where N denotes the total particle number.

Plugging the above notations into equations (1.3)-(1.5), and then removing $\sim$ from the notations, we obtain the following dimensionless form

$$
\begin{aligned}
i\frac{\partial\psi(\mathbf{x},t)}{\partial t} &= -\frac{1}{2}\nabla^2\psi(\mathbf{x},t) + V_1(\mathbf{x})\psi(\mathbf{x},t) + \left[\beta_{11}|\psi(\mathbf{x},t)|^2 + \beta_{12}|\phi(\mathbf{x},t)|^2\right]\psi(\mathbf{x},t) \\
&\quad + \left(gC(t) + \frac{\Omega}{2}\right)\phi(\mathbf{x},t) + \delta_1\psi(\mathbf{x},t), \quad\quad\quad\quad\quad (2.1) \\
i\frac{\partial\phi(\mathbf{x},t)}{\partial t} &= -\frac{1}{2}\nabla^2\phi(\mathbf{x},t) + V_2(\mathbf{x})\phi(\mathbf{x},t) + \left[\beta_{21}|\psi(\mathbf{x},t)|^2 + \beta_{22}|\phi(\mathbf{x},t)|^2\right]\phi(\mathbf{x},t) \\
&\quad + \left(g\bar{C}(t) + \frac{\Omega}{2}\right)\psi(\mathbf{x},t) + \delta_2\phi(\mathbf{x},t), \quad\quad\quad\quad\quad (2.2) \\
i\frac{\partial C(t)}{\partial t} &= \int_{\mathbb{R}^3} g\bar{\phi}(\mathbf{x},t)\psi(\mathbf{x},t)d\mathbf{x} + vC(t), \quad\quad\quad\quad\quad\quad\quad (2.3)
\end{aligned}
$$

where $\beta_{k,l} = \frac{4\pi a_{k,l} N}{a_0}$, $g = \frac{\hat{g}\sqrt{N}}{\omega_{x,1}}$, $v = \frac{\hat{v}}{\omega_{x,1}}$, $\delta_k = \frac{\hat{\delta}_k}{\omega_{x,1}}$, $\Omega = \frac{\hat{\Omega}}{\omega_{x,1}}$ and

$$V_k(\mathbf{x}) = \frac{1}{2}\left[\gamma_{x,k}^2 x^2 + \gamma_{y,k}^2 y^2 + \gamma_{z,k}^2 z^2\right], \ k = 1, 2,$$

with $\gamma_{\alpha,k} = \frac{\omega_{\alpha,k}}{\omega_{x,1}}$ ($\alpha = x, y, z$).

2.2 Reduction to lower dimensions

In this section we reduce the dimensionless coupled equations (2.1)-(2.3) into two-dimensional coupled equations and one-dimensional coupled equations.

2.2.1 Reduction to 2D

If the condensation is disk-shaped, i.e. $\omega_{x,1} \approx \omega_{y,1}$, $\omega_{z,1} \gg \omega_{x,1}$, $\omega_{x,1} \approx \omega_{x,2}$, $\omega_{x,1} \approx \omega_{y,2}$, $\omega_{z,2} \gg \omega_{x,1}$, then the three dimensional GPEs could be reduced to two-dimensional GPEs under an assumption that the time evolution could not cause excitation along the z-axis. Compared with those along x-axis and y-axis, the excitation along z-axis has much larger energy, so we might set

$$\psi(x, y, z, t) = \psi_1(x, y, t)\psi_h(z), \tag{2.4}$$

$$\phi(x, y, z, t) = \phi_1(x, y, t)\phi_h(z), \tag{2.5}$$

where $\psi_h(z) = (\frac{\gamma_{z,1}}{\pi})^{\frac{1}{4}}e^{-\frac{\gamma_{z,1}}{2}z^2}$, $\phi_h(z) = (\frac{\gamma_{z,2}}{\pi})^{\frac{1}{4}}e^{-\frac{\gamma_{z,2}}{2}z^2}$. We plug (2.4)-(2.5) into (2.1),

$$
\begin{aligned}
i\frac{\partial\psi_1}{\partial t}\psi_h &= -\frac{1}{2}\Delta\psi_1\psi_h - \frac{1}{2}\psi_1(\psi_h)_{zz} + V_1(\mathbf{x})\psi_1\psi_h + (\beta_{11}|\psi_1|^2|\psi_h|^2 \\
&\quad + \beta_{12}|\phi_1|^2|\phi_h|^2)\psi_1\psi_h + \delta_1\psi_1\psi_h.
\end{aligned}
\tag{2.6}
$$

Multiplying (2.6) by ψ_h and integrating it with respect to z, we can obtain a new function via some calculations

$$
\begin{aligned}
i\frac{\partial\psi_1(\mathbf{x}, t)}{\partial t} &= -\frac{1}{2}\nabla^2\psi_1(\mathbf{x}, t) + V_1(\mathbf{x})\psi_1(\mathbf{x}, t) + \left[\tilde{\beta}_{11}|\psi_1(\mathbf{x}, t)|^2 + \tilde{\beta}_{12}|\phi_1(\mathbf{x}, t)|^2\right]\psi_1(\mathbf{x}, t) \\
&\quad + (gC(t) + \frac{\Omega}{2})\lambda_1\phi_1(\mathbf{x}, t) + (\delta_1 + \lambda_2)\psi_1(\mathbf{x}, t),
\end{aligned}
\tag{2.7}
$$

where we denote $\tilde{\beta}_{11} = \beta_{11}\sqrt{\frac{\gamma_{z,1}}{2\pi}}$, $\tilde{\beta}_{12} = \beta_{12}\sqrt{\frac{(\gamma_{z,1}\gamma_{z,2})}{\pi(\gamma_{z,1}+\gamma_{z,2})}}$, $\lambda_1 = \frac{(4\gamma_{z,1}\gamma_{z,2})^{\frac{1}{4}}}{\sqrt{\gamma_{z,1}+\gamma_{z,2}}}$, $\lambda_2 = \int_{\mathbb{R}}\left[-\frac{1}{2}(\psi_h(z)_{zz}\psi_h(z)) + \frac{\gamma_{z,1}^2}{2}z^2\psi_h(z)^2\right]dz = \frac{3}{4}\gamma_{z,1}$.

Similarly, we can obtain two-dimensional coupled equations from (2.2)-(2.3) by setting $\tilde{\beta}_{22} = \beta_{22}\sqrt{\frac{\gamma_{z,2}}{2\pi}}$, $\tilde{\beta}_{21} = \beta_{21}\sqrt{\frac{(\gamma_{z,1}\gamma_{z,2})}{\pi(\gamma_{z,1}+\gamma_{z,2})}}$, $\lambda_3 = \frac{3}{4}\gamma_{z,2}$,

$$i\frac{\partial\phi_1(\mathbf{x},t)}{\partial t} = -\frac{1}{2}\nabla^2\phi_1(\mathbf{x},t) + V_2(\mathbf{x})\phi_1(\mathbf{x},t) + \left[\tilde{\beta}_{21}|\psi_1(\mathbf{x},t)|^2 + \tilde{\beta}_{22}|\phi_1(\mathbf{x},t)|^2\right]\phi_1(\mathbf{x},t)$$
$$+(g\bar{C}(t) + \frac{\Omega}{2})\lambda_1\psi_1(\mathbf{x},t) + (\delta_2 + \lambda_3)\phi_1(\mathbf{x},t), \tag{2.8}$$

$$i\frac{\partial C(t)}{\partial t} = \int_{\mathbb{R}^2} g\lambda_1\bar{\phi}_1(\mathbf{x},t)\psi_1(\mathbf{x},t)d\mathbf{x} + vC(t). \tag{2.9}$$

Here, $V_1(\mathbf{x}) = V_2(\mathbf{x}) = \frac{1}{2}(x^2 + y^2)$.

2.2.2 Reduction to 1D

If $\omega_{x,1} \approx \omega_{x,2}$, $\omega_{z,1} \gg \omega_{x,1}$, $\omega_{y,1} \gg \omega_{x,1}$, $\omega_{y,2} \gg \omega_{x,1}$, $\omega_{z,2} \gg \omega_{x,1}$, we set

$$\psi(x,y,z,t) = \psi_1(x,t)\psi_{h_1}(y)\psi_{h_2}(z), \tag{2.10}$$

$$\phi(x,y,z,t) = \phi_1(x,t)\phi_{h_1}(y)\phi_{h_2}(z), \tag{2.11}$$

where $\psi_{h_1}(y) = (\frac{\gamma_{y,1}}{\pi})^{\frac{1}{4}}e^{-\frac{\gamma_{y,1}}{2}y^2}$, $\phi_{h_1}(y) = (\frac{\gamma_{y,2}}{\pi})^{\frac{1}{4}}e^{-\frac{\gamma_{y,2}}{2}y^2}$, $\psi_{h_2}(z) = (\frac{\gamma_{z,1}}{\pi})^{\frac{1}{4}}e^{-\frac{\gamma_{z,1}}{2}z^2}$, $\phi_{h_2}(z) = (\frac{\gamma_{z,2}}{\pi})^{\frac{1}{4}}e^{-\frac{\gamma_{z,2}}{2}z^2}$. Similar to 2D deduction, if we substitute (2.10) and (2.11) into (2.1)-(2.3), we obtain one-dimensional coupled equations

$$i\frac{\partial\psi_1(x,t)}{\partial t} = -\frac{1}{2}\nabla^2\psi_1(x,t) + V_1(x)\psi_1(x,t) + \left[\tilde{\beta}_{11}|\psi_1(x,t)|^2 + \tilde{\beta}_{12}|\phi_1(x,t)|^2\right]\psi_1(x,t)$$
$$+(gC(t) + \frac{\Omega}{2})\lambda_1\phi_1(x,t) + (\delta_1 + \lambda_2)\psi_1(x,t), \tag{2.12}$$

$$i\frac{\partial\phi_1(x,t)}{\partial t} = -\frac{1}{2}\nabla^2\phi_1(x,t) + V_2(x)\phi_1(x,t) + \left[\tilde{\beta}_{21}|\psi_1(x,t)|^2 + \tilde{\beta}_{22}|\phi_1(x,t)|^2\right]\phi_1(x,t)$$
$$+(g\bar{C}(t) + \frac{\Omega}{2})\lambda_1\psi_1(x,t) + (\delta_2 + \lambda_3)\phi_1(x,t), \tag{2.13}$$

$$i\frac{\partial C(t)}{\partial t} = \int_{\mathbb{R}} g\lambda_1\bar{\phi}_1(x,t)\psi_1(x,t)dx + vC(t), \tag{2.14}$$

where $\tilde{\beta}_{11} = \frac{\sqrt{\gamma_{y,1}\gamma_{z,1}}}{2\pi}\beta_{11}$, $\tilde{\beta}_{12} = \frac{\sqrt{\gamma_{y,1}\gamma_{y,2}\gamma_{z,1}\gamma_{z,2}}}{\pi\sqrt{(\gamma_{y,1}+\gamma_{y,2})(\gamma_{z,1}+\gamma_{z,2})}}\beta_{12}$, $\tilde{\beta}_{22} = \frac{\sqrt{\gamma_{y,2}\gamma_{z,2}}}{2\pi}\beta_{22}$, $\tilde{\beta}_{21} = \frac{\sqrt{\gamma_{y,1}\gamma_{y,2}\gamma_{z,1}\gamma_{z,2}}}{\pi\sqrt{(\gamma_{y,1}+\gamma_{y,2})(\gamma_{z,1}+\gamma_{z,2})}}\beta_{21}$, $\lambda_1 = \frac{2(\gamma_{y,1}\gamma_{y,2}\gamma_{z,1}\gamma_{z,2})^{\frac{1}{4}}}{\sqrt{(\gamma_{y,1}+\gamma_{y,2})(\gamma_{z,1}+\gamma_{z,2})}}$, $\lambda_2 = \frac{3}{4}(\gamma_{y,1}+\gamma_{z,1})$, $\lambda_3 = \frac{3}{4}(\gamma_{y,2}+$

$\gamma_{z,2}$), and $V_1(x) = V_2(x) = \frac{1}{2}x^2$.

2.3 The general model

To sum up, the coupled equations for the two-component BEC trapped in optical resonators can be written as

$$
\begin{aligned}
i\frac{\partial\psi(\mathbf{x},t)}{\partial t} &= -\frac{1}{2}\nabla^2\psi(\mathbf{x},t) + V_1(\mathbf{x})\psi(\mathbf{x},t) + [\beta_{11}|\psi(\mathbf{x},t)|^2 + \beta_{12}|\phi(\mathbf{x},t)|^2]\psi(\mathbf{x},t) \\
&\quad + (gC(t) + \frac{\Omega}{2})\phi(\mathbf{x},t) + \delta_1\psi(\mathbf{x},t), \tag{2.15}
\end{aligned}
$$

$$
\begin{aligned}
i\frac{\partial\phi(\mathbf{x},t)}{\partial t} &= -\frac{1}{2}\nabla^2\phi(\mathbf{x},t) + V_2(\mathbf{x})\phi(\mathbf{x},t) + [\beta_{21}|\psi(\mathbf{x},t)|^2 + \beta_{22}|\phi(\mathbf{x},t)|^2]\phi(\mathbf{x},t) \\
&\quad + (g\bar{C}(t) + \frac{\Omega}{2})\psi(\mathbf{x},t) + \delta_2\phi(\mathbf{x},t), \tag{2.16}
\end{aligned}
$$

$$
i\frac{\partial C(t)}{\partial t} = \int_{\mathbb{R}^d} g\bar{\phi}(\mathbf{x},t)\psi(\mathbf{x},t)d\mathbf{x} + vC(t), \quad \mathbf{x} \in \mathbb{R}^d, t > 0, \tag{2.17}
$$

where d=1, 2, 3.

2.4 Some conservation properties

There are several invariants governed by the coupled equations (2.15)-(2.17) for coupling BEC trapped in the optical cavity. The total mass conservation and energy conservation are two of the most important invariants.

2.4.1 Mass conservation

We define the mass of the two condensates respectively as

$$
N(\psi(\mathbf{x},t)) = \int_{\mathbb{R}^d} |\psi(\mathbf{x},t)|^2 d\mathbf{x}, \quad N(\phi(\mathbf{x},t)) = \int_{\mathbb{R}^d} |\phi(\mathbf{x},t)|^2 d\mathbf{x}, \quad \mathbf{x} \in \mathbb{R}^d, \ t > 0.
$$

Lemma 2.4.1. *Suppose that $\psi(\mathbf{x},t)$, $\phi(\mathbf{x},t)$, are the solutions of (2.15)-(2.17), then the total mass $N(\psi) + N(\phi)$ is conserved.*

Proof: First we multiply (2.15) by $\bar{\psi}$ and integrate it in $\mathbb{R}^d$ with respect to $\mathbf{x}$. By integrating by parts, we have

$$i \int_{\mathbb{R}^d} \frac{\partial \psi(\mathbf{x},t)}{\partial t} \bar{\psi}(\mathbf{x},t) d\mathbf{x} = \int_{\mathbb{R}^d} \Big\{ -\frac{1}{2} \triangle \psi(\mathbf{x},t) \bar{\psi}(\mathbf{x},t) + \big[\beta_{11} |\psi(\mathbf{x},t)|^2 + \beta_{12} |\phi(\mathbf{x},t)|^2 \big] |\psi(\mathbf{x},t)|^2$$

$$+ V_1(\mathbf{x}) |\psi(\mathbf{x},t)|^2 + (gC(t) + \frac{\Omega}{2}) \phi(\mathbf{x},t) \bar{\psi}(\mathbf{x},t) + \delta_1 |\psi(\mathbf{x},t)|^2 \Big\} d\mathbf{x},$$

$$= \int_{\mathbb{R}^d} \Big\{ \frac{1}{2} |\triangledown \psi(\mathbf{x},t)|^2 + V_1(\mathbf{x}) |\psi(\mathbf{x},t)|^2 + (gC(t) + \frac{\Omega}{2}) \phi(\mathbf{x},t) \bar{\psi}(\mathbf{x},t)$$

$$+ \big[\beta_{11} |\psi(\mathbf{x},t)|^2 + \beta_{12} |\phi(\mathbf{x},t)|^2 \big] |\psi(\mathbf{x},t)|^2 + \delta_1 |\psi(\mathbf{x},t)|^2 \Big\} d\mathbf{x}. \qquad (2.18)$$

Taking a conjugate of (2.15), we multiply it by ψ. Similarly integrating by parts, we have:

$$i \int_{\mathbb{R}^d} \frac{\partial \bar{\psi}(\mathbf{x},t)}{\partial t} \psi(\mathbf{x},t) d\mathbf{x} = \int_{\mathbb{R}^d} \Big\{ \frac{1}{2} \triangle \bar{\psi}(\mathbf{x},t) \psi(\mathbf{x},t) - \big[\beta_{11} |\psi(\mathbf{x},t)|^2 + \beta_{12} |\phi(\mathbf{x},t)|^2 \big] |\psi(\mathbf{x},t)|^2$$

$$- V_1(\mathbf{x}) |\psi(\mathbf{x},t)|^2 - (g\bar{C}(t) + \frac{\Omega}{2}) \bar{\phi}(\mathbf{x},t) \psi(\mathbf{x},t) - \delta_1 |\psi(\mathbf{x},t)|^2 \Big\} d\mathbf{x},$$

$$= - \int_{\mathbb{R}^d} \Big\{ \frac{1}{2} |\triangledown \psi(\mathbf{x},t)|^2 + V_1(\mathbf{x}) |\psi(\mathbf{x},t)|^2 + (g\bar{C}(t) + \frac{\Omega}{2}) \bar{\phi}(\mathbf{x},t) \psi(\mathbf{x},t)$$

$$+ \big[\beta_{11} |\psi(\mathbf{x},t)|^2 + \beta_{12} |\phi(\mathbf{x},t)|^2 \big] |\psi(\mathbf{x},t)|^2 + \delta_1 |\psi(\mathbf{x},t)|^2 \Big\} d\mathbf{x}. \qquad (2.19)$$

Summing up both (2.18) and (2.19), we can get:

$$i \frac{\partial}{\partial t} \int_{\mathbb{R}^d} |\psi|^2 d\mathbf{x} = \int_{\mathbb{R}^d} \Big[(gC + \frac{\Omega}{2}) \phi \bar{\psi} - (g\bar{C} + \frac{\Omega}{2}) \bar{\phi} \psi \Big] d\mathbf{x}.$$

Similarly, from (2.16) we can get

$$i \frac{\partial}{\partial t} \int_{\mathbb{R}^d} |\phi|^2 d\mathbf{x} = \int_{\mathbb{R}^d} \Big[(g\bar{C} + \frac{\Omega}{2}) \bar{\phi} \psi - (gC + \frac{\Omega}{2}) \phi \bar{\psi} \Big] d\mathbf{x}.$$

Thus, we may easily obtain

$$i \frac{\partial}{\partial t} \int_{\mathbb{R}^d} \Big[|\psi|^2 + |\phi|^2 \Big] d\mathbf{x} = 0,$$

which indicates that the total mass, i.e., $N(\psi) + N(\phi)$ of two condensates is conserved.

2.4.2 Energy conservation

Another important invariant is the energy. The energy is defined as

$$E(t) := E(\psi(\mathbf{x}, t), \phi(\mathbf{x}, t), C(t)) = E_1(t) + E_2(t) + v|C(t)|^2, \tag{2.20}$$

where

$$
\begin{aligned}
E_1(t) \ = \ & \int_{\mathbb{R}^d} \left[\frac{1}{2} |\nabla \psi(\mathbf{x}, t)|^2 + V_1(\mathbf{x}) |\psi(\mathbf{x}, t)|^2 + (gC(t) + \frac{\Omega}{2}) \phi(\mathbf{x}, t) \bar{\psi}(\mathbf{x}, t) \right. \\
& \left. + \frac{1}{2} \left[\beta_{11} |\psi(\mathbf{x}, t)|^2 + \beta_{12} |\phi(\mathbf{x}, t)|^2 \right] |\psi(\mathbf{x}, t)|^2 + \delta_1 |\psi(\mathbf{x}, t)|^2 \right] d\mathbf{x}, \tag{2.21}
\end{aligned}
$$

$$
\begin{aligned}
E_2(t) \ = \ & \int_{\mathbb{R}^d} \left[\frac{1}{2} |\nabla \phi(\mathbf{x}, t)|^2 + V_2(\mathbf{x}) |\phi(\mathbf{x}, t)|^2 + (g\bar{C}(t) + \frac{\Omega}{2}) \bar{\phi}(\mathbf{x}, t) \psi(\mathbf{x}, t) \right. \\
& \left. + \frac{1}{2} \left[\beta_{21} |\psi(\mathbf{x}, t)|^2 + \beta_{22} |\phi(\mathbf{x}, t)|^2 \right] |\phi(\mathbf{x}, t)|^2 + \delta_2 |\phi(\mathbf{x}, t)|^2 \right] d\mathbf{x}, \tag{2.22}
\end{aligned}
$$

Lemma 2.4.2. *Suppose that $\psi(\mathbf{x}, t)$, $\phi(\mathbf{x}, t)$, are the solutions of (2.15)-(2.17) and $\beta_{12} = \beta_{21}$, then the energy (2.20) is conserved.*

Proof: Differentiating (2.20) with respect to time t, we can get

$$\frac{dE}{dt} = \frac{dE_1}{dt} + \frac{dE_2}{dt} + v \frac{d|C|^2}{dt}, \tag{2.23}$$

where

$$
\begin{aligned}
\frac{dE_1}{dt} \ = \ & \int_{\mathbb{R}^d} \left[-\frac{1}{2} (\triangle \psi \partial_t \bar{\psi} + \partial_t \psi \triangle \bar{\psi}) + \frac{1}{2} \left[\beta_{11} (\partial_t \psi \bar{\psi} + \psi \partial_t \bar{\psi}) + \beta_{12} (\partial_t \phi \bar{\phi} + \phi \partial_t \bar{\phi}) \right] |\psi|^2 \right. \\
& + \frac{1}{2} \left[\beta_{11} |\psi|^2 + \beta_{12} |\phi|^2 \right] (\partial_t \psi \bar{\psi} + \psi \partial_t \bar{\psi}) + (V_1 + \delta_1)(\partial_t \psi \bar{\psi} + \psi \partial_t \bar{\psi}) + g \frac{dC}{dt} \phi \bar{\psi} \\
& \left. + (gC + \frac{\Omega}{2})(\partial_t \phi \bar{\psi} + \phi \partial_t \bar{\psi}) \right] d\mathbf{x}, \tag{2.24}
\end{aligned}
$$

and

$$
\begin{aligned}
\frac{dE_2}{dt} &= \int_{\mathbb{R}^d} \left[-\frac{1}{2}(\triangle\phi\partial_t\bar\phi + \partial_t\phi\triangle\bar\phi) + \frac{1}{2}\left[\beta_{21}(\partial_t\psi\bar\psi + \psi\partial_t\bar\psi) + \beta_{22}(\partial_t\phi\bar\phi + \phi\partial_t\bar\phi)\right]|\phi|^2 \right. \\
&\quad + \frac{1}{2}\left[\beta_{21}|\psi|^2 + \beta_{22}|\phi|^2\right](\partial_t\phi\bar\phi + \phi\partial_t\bar\phi) + (V_2 + \delta_2)(\partial_t\phi\bar\phi + \phi\partial_t\bar\phi) + g\frac{d\bar C}{dt}\psi\bar\phi \\
&\quad \left. + (g\bar C + \frac{\Omega}{2})(\partial_t\bar\phi\psi + \bar\phi\partial_t\psi) \right] d\mathbf{x}.
\end{aligned}
\tag{2.25}
$$

Since $\beta_{12} = \beta_{21}$ and taking into consideration of equations (2.15)-(2.16), we can get

$$
\begin{aligned}
\frac{dE_1}{dt} + \frac{dE_2}{dt} &= \int_{\mathbb{R}^d} \left[g\bar\phi\psi\frac{d\bar C}{dt} + g\phi\bar\psi\frac{dC}{dt} \right] d\mathbf{x} \\
&= \left(\int_{\mathbb{R}^d} g\bar\phi\psi d\mathbf{x} + vC \right)\frac{d\bar C}{dt} - vC\frac{d\bar C}{dt} + \left(\int g\phi\bar\psi d\mathbf{x} + v\bar C \right)\frac{dC}{dt} - v\bar C\frac{dC}{dt} \\
&= -v\frac{d|C|^2}{dt}.
\end{aligned}
\tag{2.26}
$$

Thus we can finally get

$$
\frac{dE}{dt} = 0,
\tag{2.27}
$$

which indicates the energy (2.20) is conserved.

Chapter 3

Ground state of coupling BEC in optical resonators

In this chapter, we study how to compute the ground state of the coupling BEC trapped in optical resonators. First we present the definition of the ground state. Next we propose a gradient flow with discrete normalization for computing the ground state and discretize the gradient flow with a backward Euler Sine pseudospectral method. Finally we apply the proposed method to investigate the ground state solution of coupling BEC in optical resonators in 1D and 2D, respectively.

3.1   Stationary solutions

To find stationary solutions of (2.15)-(2.17), we write

$$\psi(\mathbf{x}, t) = e^{-i\mu t}\psi_s(\mathbf{x}), \quad \phi(\mathbf{x}, t) = e^{-i\mu t}\phi_s(\mathbf{x}), \quad C(t) = c_s \in \mathbb{C}, \qquad (3.1)$$

where μ is the chemical potential of the BEC, $\psi_s(\mathbf{x})$ and $\phi_s(\mathbf{x})$ are complex and independent of time. Inserting (3.1) into (2.15)-(2.17) gives us the following time-independent

equations for $\psi_s(\mathbf{x})$, $\phi_s(\mathbf{x})$ and c_s

$$
\begin{aligned}
\mu\psi_s(\mathbf{x}) = {}& -\frac{1}{2}\nabla^2\psi_s(\mathbf{x}) + V_1(\mathbf{x})\psi_s(\mathbf{x}) + \left[\beta_{11}|\psi_s(\mathbf{x})|^2 + \beta_{12}|\phi_s(\mathbf{x})|^2\right]\psi_s(\mathbf{x}) \\
& + (gc_s + \frac{\Omega}{2})\phi_s(\mathbf{x}) + \delta_1\psi_s(\mathbf{x}), && (3.2)
\end{aligned}
$$

$$
\begin{aligned}
\mu\phi_s(\mathbf{x}) = {}& -\frac{1}{2}\nabla^2\phi_s(\mathbf{x}) + V_2(\mathbf{x})\phi_s(\mathbf{x}) + \left[\beta_{21}|\psi_s(\mathbf{x})|^2 + \beta_{22}|\phi_s(\mathbf{x})|^2\right]\phi_s(\mathbf{x}) \\
& + (g\bar{c}_s + \frac{\Omega}{2})\psi_s(\mathbf{x}) + \delta_2\phi_s(\mathbf{x}), && (3.3)
\end{aligned}
$$

$$
c_s = -\frac{g}{v}\int_{\mathbb{R}^d}\bar{\phi}_s(\mathbf{x})\psi_s(\mathbf{x})d\mathbf{x}, \qquad (3.4)
$$

while $\psi_s(\mathbf{x})$, $\phi_s(\mathbf{x})$ must satisfy

$$
\int_{\mathbb{R}^d}\left(|\psi_s(\mathbf{x})|^2 + |\phi_s(\mathbf{x})|^2\right)\,d\mathbf{x} = 1. \qquad (3.5)
$$

This turns out to be a nonlinear eigenvalue problem with one constraint and the chemical potential μ can be computed from its corresponding eigenfunctions $\psi_s(\mathbf{x})$, $\phi_s(\mathbf{x})$. We may compute μ by

$$
\begin{aligned}
\mu(\psi_s, \phi_s, c_s) = \int_{\mathbb{R}^d}\Big[& \tfrac{1}{2}(|\nabla\psi_s(\mathbf{x})|^2 + |\nabla\phi_s(\mathbf{x})|^2) + [\beta_{11}|\psi_s(\mathbf{x})|^2 + \beta_{12}|\phi_s(\mathbf{x})|^2]|\psi_s(\mathbf{x})|^2 \\
& + [\beta_{21}|\psi_s(\mathbf{x})|^2 + \beta_{22}|\phi_s(\mathbf{x})|^2]|\phi_s(\mathbf{x})|^2 + (V_1(\mathbf{x}) + \delta_1)|\psi_s(\mathbf{x})|^2 + (V_2(\mathbf{x}) \\
& + \delta_2)|\phi_s(\mathbf{x})|^2 + (\tfrac{\Omega}{2} + gc_s)\phi_s(\mathbf{x})\bar{\psi}_s(\mathbf{x}) + (\tfrac{\Omega}{2} + g\bar{c}_s)\bar{\phi}_s(\mathbf{x})\psi_s(\mathbf{x})\Big]d\mathbf{x}. \quad (3.6)
\end{aligned}
$$

There are many solutions to the nonlinear eigenvalue problem (3.2)-(3.4) with the constraint (3.5), among which the ground state solution is of most interest. In the coming sections, we will discuss how to define the ground state solution and how to compute the ground state solution.

3.2 Ground state

The ground state solution for the coupling BEC trapped in optical resonators $(\psi_{gs}(\mathbf{x})$, $\phi_{gs}(\mathbf{x}), c_{gs})$ can be found by minimizing the energy $E(\psi, \phi, C)$ under the constraint (3.5), i.e.

(A) Find $(\phi_{gs}, \phi_{gs}, c_{gs}) \in S$ such that

$$E(\psi_{gs}, \phi_{gs}, c_{gs}) = \min_{(\psi,\phi,C)\in S} E(\psi, \phi, C), \tag{3.7}$$

where the set S is defined as

$$S = \{(\psi, \phi, C) \mid \| \phi \|_2^2 + \| \psi \|_2^2 = 1, C \in \mathbb{C}, E(\psi, \phi, C) < \infty\}.$$

If we define

$$\mu_{gs} = \mu(\psi_{gs}, \phi_{gs}, c_{gs}),$$

it is easy to see that $(\mu_{gs}, \psi_{gs}, \phi_{gs}, c_{gs})$ is a solution of nonlinear eigenvalue problem (3.2)-(3.4) with the constraint (3.5).

Remark:

Since $c_{gs} = -\frac{g}{v} \int_{\mathbb{R}^d} \bar{\phi}_{gs} \psi_{gs} \, d\mathbf{x}$, we may reformulate the definition of the ground state solution for the coupling BEC trapped in optical resonators as follows:

(B) Find $(\psi_{gs}, \phi_{gs}) \in \tilde{S}$ such that

$$\tilde{E}(\psi_{gs}, \phi_{gs}) = \min_{(\psi,\phi)\in\tilde{S}} \tilde{E}(\psi, \phi), \tag{3.8}$$

where the set $\tilde{S}$ is defined as

$$\tilde{S} = \{(\psi, \phi) \mid \| \phi \|_2^2 + \| \psi \|_2^2 = 1, \tilde{E}(\psi, \phi) < \infty\}.$$

Here the energy is defined as

$$
\begin{aligned}
\tilde{E}(\psi, \phi) &= \int_{\mathbb{R}^d} \left[\frac{1}{2}(| \bigtriangledown \psi(\mathbf{x})|^2 + | \bigtriangledown \phi(\mathbf{x})|^2) + (V_1(\mathbf{x}) + \delta_1)|\psi(\mathbf{x})|^2 + (V_2(\mathbf{x}) + \delta_2)|\phi(\mathbf{x})|^2 \right. \\
&+ \frac{1}{2} \left[\beta_{11}|\psi(\mathbf{x})|^2 + \beta_{12}|\phi(\mathbf{x})|^2\right] |\psi(\mathbf{x})|^2 + \frac{1}{2} \left[\beta_{21}|\psi(\mathbf{x})|^2 + \beta_{22}|\phi(\mathbf{x})|^2\right] |\phi(\mathbf{x})|^2 \\
&+ \left. \frac{\Omega}{2}\phi(\mathbf{x})\bar{\psi}(\mathbf{x}) + \frac{\Omega}{2}\bar{\phi}(\mathbf{x})\psi(\mathbf{x}) \right] d\mathbf{x} - \frac{g^2}{v}| \int_{\mathbb{R}^d} \bar{\phi}\psi d\mathbf{x}|^2. \tag{3.9}
\end{aligned}
$$

Any eigenfunction pair $\psi_s(\mathbf{x})$ and $\phi_s(\mathbf{x})$ of (3.2)-(3.3) along with its corresponding c_s found from (3.4) whose energy greater than $E(\psi_{gs}, \phi_{gs}, c_{gs})$ is usually called as excited

states in the physics literature. In this thesis, we are mainly interested in computing the ground state solutions, which will be discussed in the next section.

3.3 Numerical method

In this section, we propose an efficient numerical method—gradient flow with discrete normalization to compute the ground state, i.e. the minimizer of (3.7).

3.3.1 Continuous normalized gradient flow

In order to compute the ground state, we construct the following continuous normalized gradient flow (CNGF):

$$
\begin{aligned}
\frac{\partial \psi(\mathbf{x},t)}{\partial t} &= \frac{1}{2}\nabla^2\psi(\mathbf{x},t) - V_1(\mathbf{x})\psi(\mathbf{x},t) - \left[\beta_{11}|\psi(\mathbf{x},t)|^2 + \beta_{12}|\phi(\mathbf{x},t)|^2\right]\psi(\mathbf{x},t) - \delta_1\psi(\mathbf{x},t) \\
&\quad - (gC(t) + \frac{\Omega}{2})\phi(\mathbf{x},t) + \frac{\mu(t)}{\parallel\psi(\mathbf{x},t)\parallel^2 + \parallel\phi(\mathbf{x},t)\parallel^2}\psi(\mathbf{x},t), \qquad (3.10)
\end{aligned}
$$

$$
\begin{aligned}
\frac{\partial \phi(\mathbf{x},t)}{\partial t} &= \frac{1}{2}\nabla^2\phi(\mathbf{x},t) - V_2(\mathbf{x})\phi(\mathbf{x},t) - \left[\beta_{21}|\psi(\mathbf{x},t)|^2 + \beta_{22}|\phi(\mathbf{x},t)|^2\right]\phi(\mathbf{x},t) - \delta_2\phi(\mathbf{x},t) \\
&\quad - (g\bar{C}(t) + \frac{\Omega}{2})\psi(\mathbf{x},t) + \frac{\mu(t)}{\parallel\psi(\mathbf{x},t)\parallel^2 + \parallel\phi(\mathbf{x},t)\parallel^2}\phi(\mathbf{x},t), \qquad (3.11)
\end{aligned}
$$

$$
\frac{\partial C(t)}{\partial t} = -\int_{\mathbb{R}^d} g\bar{\phi}(\mathbf{x},t)\psi(\mathbf{x},t)d\mathbf{x} - vC(t), \qquad (3.12)
$$

where $\mu(t)$ is chosen such that the above CNGF is mass conservative and $\mu(t)$ can be defined as

$$
\mu(t) := \mu(\psi(\mathbf{x},t), \phi(\mathbf{x},t), C(t)),
$$

which is given in (3.6) with $\psi_s = \psi(\mathbf{x},t)$, $\phi_s = \phi(\mathbf{x},t)$, $c_s = C(\mathbf{x},t)$. For the CNGF, we have

Lemma 3.3.1. *For any given initial data*

$$
\psi(\mathbf{x},t=0), \ \phi(\mathbf{x},t=0), \ C(t=0), \qquad (3.13)
$$

the CNGF (3.10)-(3.12) satisfies

$$
||\psi(\mathbf{x},t)||^2 + ||\phi(\mathbf{x},t)||^2 = ||\psi(\mathbf{x},t=0)||^2 + ||\phi(\mathbf{x},t=0)||^2,
$$

i.e. the CNGF (3.10)-(3.12) is mass conservative and furthermore,

$$E(\psi(\mathbf{x}, t), \psi(\mathbf{x}, t), C(t)) \le E(\psi(\mathbf{x}, s), \psi(\mathbf{x}, s), C(s)), \; for \; any \; t > s,$$

i.e., the energy is diminishing.

Proof: Similar to [63], taking the time derivative of the total mass and the energy, we can find

$$\frac{d \left(||\psi(\mathbf{x}, t)||^2 + ||\phi(\mathbf{x}, t)||^2 \right)}{dt} = 0,$$

and

$$\frac{dE}{dt} = -2 \int_{\mathbb{R}^d} \left(|\partial_t \psi|^2 + |\partial_t \phi|^2 \right) \; d\mathbf{x} - 2|\frac{dC}{dt}|^2 \le 0,$$

which imply that the CNGF has the property of mass conservative and the energy diminishing.

From the CNGF (3.10)-(3.12), we may get that as $t \to \infty$, $\psi(\mathbf{x}, t)$, $\phi(\mathbf{x}, t)$ and $C(t)$ approach to steady a state solution, which is a critical point of the energy functional $E(\psi, \phi, C)$ over the unit sphere S. In addition, when the initial data in (3.13) is chosen properly, e.g. its energy is less than that of excited states, the ground state solution can be obtained from the steady state solution of (3.10)-(3.12), i.e.,

$$\psi_{gs}(\mathbf{x}) = \lim_{t \to \infty} \psi(\mathbf{x}, t), \; \psi_{gs}(\mathbf{x}) = \lim_{t \to \infty} \psi(\mathbf{x}, t), \; c_{gs} = \lim_{t \to \infty} C(t).$$

In practical calculation, if we discretize the CNGF (3.10)-(3.12) directly, we need to solve a fully nonlinear system which is very tedious in practical computation. In the next subsection, we present a more efficient way to compute the ground states.

3.3.2 Gradient flow with discrete normalization

To compute the ground state solution, we evolve the following gradient flow with discrete normalization (GFDN),

$$
\begin{aligned}
\frac{\partial \psi(\mathbf{x}, t)}{\partial t} &= \frac{1}{2} \nabla^2 \psi(\mathbf{x}, t) - V_1(\mathbf{x}) \psi(\mathbf{x}, t) - \left[\beta_{11} |\psi(\mathbf{x}, t)|^2 + \beta_{12} |\phi(\mathbf{x}, t)|^2 \right] \psi(\mathbf{x}, t) \\
&\quad - (gC(t) + \frac{\Omega}{2}) \phi(\mathbf{x}, t) - \delta_1 \psi(\mathbf{x}, t),
\end{aligned} \tag{3.14}
$$

$$\frac{\partial \phi(\mathbf{x}, t)}{\partial t} = \frac{1}{2} \nabla^2 \phi(\mathbf{x}, t) - V_2(\mathbf{x}) \phi(\mathbf{x}, t) - \left[\beta_{21} |\psi(\mathbf{x}, t)|^2 + \beta_{22} |\phi(\mathbf{x}, t)|^2 \right] \phi(\mathbf{x}, t)$$

$$- (g\bar{C}(t) + \frac{\Omega}{2}) \psi(\mathbf{x}, t) - \delta_2 \phi(\mathbf{x}, t), \tag{3.15}$$

$$\frac{\partial C(t)}{\partial t} = - \int_{\mathbb{R}^d} g\bar{\phi}(\mathbf{x}, t) \psi(\mathbf{x}, t) d\mathbf{x} - vC(t), \quad t_{n+1} > t > t_n, \tag{3.16}$$

$$\psi(\mathbf{x}, t_{n+1}) = \psi(\mathbf{x}, t_{n+1}^+) = \frac{\psi(\mathbf{x}, t_{n+1}^-)}{\sqrt{\| \psi(\mathbf{x}, t_{n+1}^-) \|_2^2 + \| \phi(\mathbf{x}, t_{n+1}^-) \|_2^2}}, \tag{3.17}$$

$$\phi(\mathbf{x}, t_{n+1}) = \phi(\mathbf{x}, t_{n+1}^+) = \frac{\phi(\mathbf{x}, t_{n+1}^-)}{\sqrt{\| \psi(\mathbf{x}, t_{n+1}^-) \|_2^2 + \| \phi(\mathbf{x}, t_{n+1}^-) \|_2^2}}, \tag{3.18}$$

with

$$\psi(\mathbf{x}, 0) = \psi_0(\mathbf{x}), \ \phi(\mathbf{x}, 0) = \phi_0(\mathbf{x}), \ C(0) = C_0, \tag{3.19}$$

where

$$\psi(\mathbf{x}, t_{n+1}^\pm) = \lim_{t \to t_{n+1}^\pm} \psi(\mathbf{x}, t), \quad \phi(\mathbf{x}, t_{n+1}^\pm) = \lim_{t \to t_{n+1}^\pm} \phi(\mathbf{x}, t). \tag{3.20}$$

Actually we can consider the gradient flow (3.14)-(3.16) as applying the steepest decent method to the energy functional $E(\psi, \phi, C)$ without constraints, and projecting the solution back onto the unit sphere S. From numerical point of view, the GFDN (3.14)-(3.16) is much easier to discretize since the gradient flow (3.14)-(3.16) can be solved via typical numerical techniques for partial differential equations.

In our calculations, we discretize the equations (3.14)-(3.15) with the backward Euler method in time and Sine pseudospectral method in space, while we discretize the equation (3.16) with the backward Euler method in time and the integral in the equation (3.16) with composite trapezoidal rule. By doing this way, we can use larger time step to reach steady state solutions while having spectral accuracy in space. We describe the detailed algorithm of the method in the next subsection.

3.3.3 A backward Euler Sine pseudospectral method

In this section, we present a backward Euler Sine pseudospectral method for discretizing the equations (3.14)-(3.16) in 1D. Extension of the method to higher dimensions is straightforward.

In the computation, we choose $\Omega_x = [a, b]$ with $|a|$, $|b|$ sufficiently large and define $\triangle t$ (> 0) as the time step. We choose the spatial mesh sizes $h_x = \triangle x > 0$ with $h_x = (b-a)/M$ (M is an even positive integers). We define grid points and time steps by

$$x_j := a + j\,h_x, \quad j = 0, 1, \cdots, M; \quad t_n := n\,\triangle t, \quad n = 0, 1, 2, \cdots. \tag{3.21}$$

Let ψ_j^n, ϕ_j^n and C^n be the numerical approximation of $\psi(x_j, t_n)$, $\phi(x_j, t_n)$ and $C(t_n)$, respectively.

We discretize the equations (3.14)-(3.15) with backward Euler method in time and Sine pseudospectral method in space. The detailed numerical scheme is as follows:

$$\frac{\tilde{\psi}_j - \psi_j^n}{\triangle t} = \frac{1}{2} D_x D_x \tilde{\psi}_j - \alpha^{(1)} \tilde{\psi}_j + F_j^n,$$

$$F_j^n = \alpha^{(1)} \psi_j^n - V_1(x_j)\psi_j^n - \beta_{11} \left|\psi_j^n\right|^2 \psi_j^n - \beta_{12} \left|\phi_j^n\right|^2 \psi_j^n - \left(gC^n + \frac{\Omega}{2}\right)\phi_j^n - \delta_1 \psi_j^n,$$

$$\frac{\tilde{\phi}_j - \phi_j^n}{\triangle t} = \frac{1}{2} D_x D_x \tilde{\phi}_j - \alpha^{(2)} \tilde{\phi}_j + G_j^n, \tag{3.22}$$

$$G_j^n = \alpha^{(2)} \phi_j^n - V_2(x_j)\phi_j^n - \beta_{21} \left|\psi_j^n\right|^2 \phi_j^n - \beta_{22} \left|\phi_j^n\right|^2 \phi_j^n - \left(g\bar{C}^n + \frac{\Omega}{2}\right)\psi_j^n - \delta_2 \phi_j^n,$$

$$\frac{C^{n+1} - C^n}{\triangle t} = -\int_{\Omega_x} g\bar{\phi}_j^{n+1} \psi_j^{n+1} dx - vC^{n+1},$$

$$\psi_j^{n+1} = \frac{\tilde{\psi}_j}{\sqrt{\|\tilde{\psi}\|^2 + \|\tilde{\phi}\|^2}}, \quad \phi_j^{n+1} = \frac{\tilde{\phi}_j}{\sqrt{\|\tilde{\psi}\|^2 + \|\tilde{\phi}\|^2}}, \quad j = 0, 1, \cdots, M, \quad n = 0, 1, \cdots,$$

$$\psi_j^0 = \psi_0(x_j), \quad \phi_j^0 = \phi_0(x_j), \quad j = 0, 1, \cdots, M,$$

$$\tilde{\psi}_0 = \tilde{\psi}_M = 0, \ \tilde{\phi}_0 = \tilde{\phi}_M = 0,$$

where the norm is defined as $\|\tilde{\phi}\|^2 = h_x \sum_{j=1}^{M-1} |\tilde{\phi}_j|^2$. $\alpha^{(1)}$ and $\alpha^{(2)}$ are stabilization parameters which are chosen such that the time step can be chosen as large as possible.

They can be defined as

$$\alpha^{(k)} = \frac{1}{2}\left(\alpha_k^{\max} + \alpha_k^{\min}\right), \quad k = 1, 2, \tag{3.23}$$

with

$$\alpha_k^{\max} = \max_{1 \le j \le M-1}\left[V_k(x_j) + \beta_{k1}\left|\psi_j^n\right|^2 + \beta_{k2}\left|\phi_j^n\right|^2\right],$$

$$\alpha_k^{\min} = \min_{1 \le j \le M-1}\left[V_k(x_j) + \beta_{k1}\left|\psi_j^n\right|^2 + \beta_{k2}\left|\phi_j^n\right|^2\right].$$

The pseudospectral operator $D_x D_x \tilde{\psi}_j$ in (3.22) is defined as

$$D_x D_x \tilde{\psi}_j = -\sum_{p=1}^{M-1}(\mu_p^2)\widehat{\tilde{\psi}}_p \sin(\mu_p(x_j - a)), \tag{3.24}$$

where

$$\mu_p = \frac{\pi p}{b - a}. \tag{3.25}$$

The pseudospectral operator $D_x D_x \tilde{\phi}_j$ can be defined in a similar way.

In the above formula (3.24), we have defined the inverse discrete Sine transform (IDST) as

$$\hat{U}_p = \frac{2}{M}\sum_{j=1}^{M-1} U_j \sin(\mu_p(x_j - a)), \quad p = 1, \cdots, M-1,$$

and the discrete Sine transform (DST) as

$$U_j = \sum_{p=1}^{M-1}\hat{U}_p \sin(\mu_p(x_j - a)), \quad j = 1, 2, \cdots, M-1,$$

if we assume $U(x_j) \equiv U_j$ for a given function $U(x)$.

3.4 Numerical results

In this section, we apply the proposed numerical method to compute the ground state solutions of coupling BEC confined in the optical cavity. In all of our computation, the

threshold of approaching steady state solutions is set as

$$\| \psi^{k+1} - \psi^k \|_\infty < 10^{-7}, \quad \| \phi^{k+1} - \phi^k \|_\infty < 10^{-7} \text{ and } |C^{k+1} - C^k| < 10^{-7},$$

for arbitrary step k.

3.4.1 Ground state solutions in 1D

Example 3.1. In this example, we show that our numerical method for computing one-dimensional ground states is reliable by choosing different arbitrary initial data:

$$
\begin{aligned}
Case\ \ 1, \quad & \psi(x,0) = \phi(x,0) = \frac{1}{\pi^{\frac{1}{4}}\sqrt{2}}e^{-\frac{x^2}{2}}, \quad C(0) = 1 + i, \\
Case\ \ 2, \quad & \psi(x,0) = \phi(x,0) = \frac{1}{\pi^{\frac{1}{4}}2^{\frac{3}{4}}}e^{-\frac{x^2}{4}}, \quad C(0) = 1 + 2i, \\
Case\ \ 3, \quad & \psi(x,0) = \frac{1}{\pi^{\frac{1}{4}}\sqrt{2}}e^{-\frac{x^2}{2}}, \quad \phi(x,0) = \frac{1}{\pi^{\frac{1}{4}}2^{\frac{3}{4}}}e^{-\frac{x^2}{4}}, \quad C(0) = 3 + i.
\end{aligned}
$$

In the computation, the following parameters are used: $V_1(x) = V_2(x) = \frac{x^2}{2}$, $\delta_1 = 0.5$, $\delta_2 = 0$, $\Omega = 1$, $g = 1$, $v = 1$ and $\beta_{11} : \beta_{12} : \beta_{21} : \beta_{22} = (1 : 0.94 : 0.94 : 0.97)\beta$ with $\beta = 100$. We set time step $\Delta t = 0.1$ and $\triangle x = 1/32$.
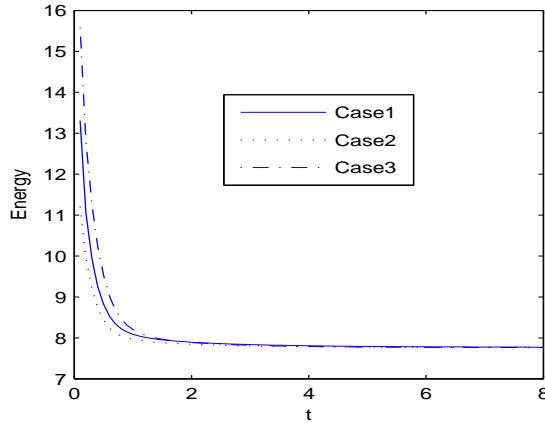
Figure 3.1: Gradient flows prepared with different initial data converge into the same steady-state solution which has the same energy.

Figure 3.1 shows us that (1) the computed normalized gradient flow has the property of energy diminishing; (2) the normalized gradient flows converge into the same ground state which has the same energy, though prepared with different data types.

Example 3.2. In this example, we show that the coupling strength g can determine the size of two condensates. In the computation, the following parameters are used: $V_1(x) = V_2(x) := V(x)$, $\delta_1 = \delta_2 = 0$, $\Omega = 0$, $v = 1$ and $\beta_{11} : \beta_{12} : \beta_{21} : \beta_{22} = (1 : 0.94 : 0.94 : 0.97)\beta$ with $\beta = 100$. The initial data is chosen as $\psi(x,0) = \phi(x,0) = \frac{1}{\pi^{\frac{1}{4}}\sqrt{2}}e^{-\frac{x^2}{2}}$, $C(0) = 1 + i$.
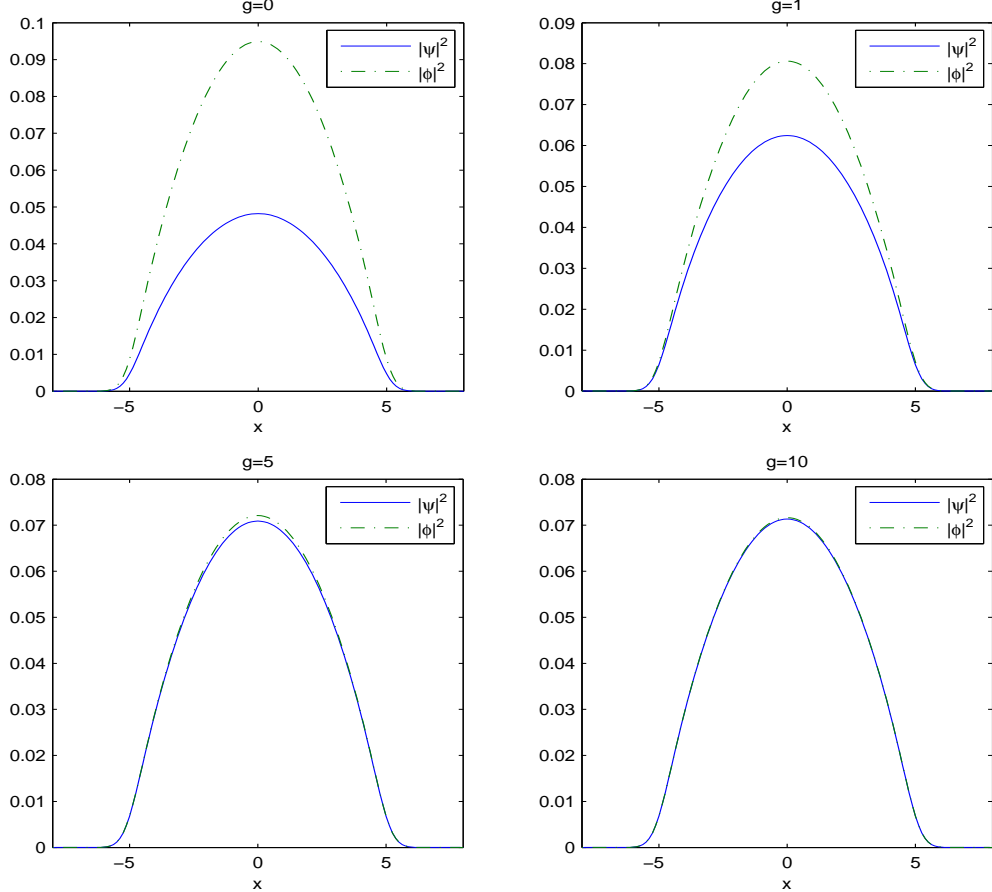
Figure 3.2: Density plots of ground states trapped in a harmonic trap with different coupling strength g in **Example 3.2**.

In the numerical calculation, the trap potential $V(x)$ can be a harmonic trap, a double-well trap or a harmonic plus optical lattice trap.

Figure 3.2 shows density plots of ground states trapped in a harmonic trap (i.e., $V(x) = \frac{x^2}{2}$) with different coupling strength g.

Figure 3.3 shows density plots of ground states trapped in a double-well trap (i.e., $V(x) = \frac{(|x|-1.5)^2}{2}$) with different coupling strength g.

Figure 3.4 shows density plots of ground states trapped in a harmonic plus optical
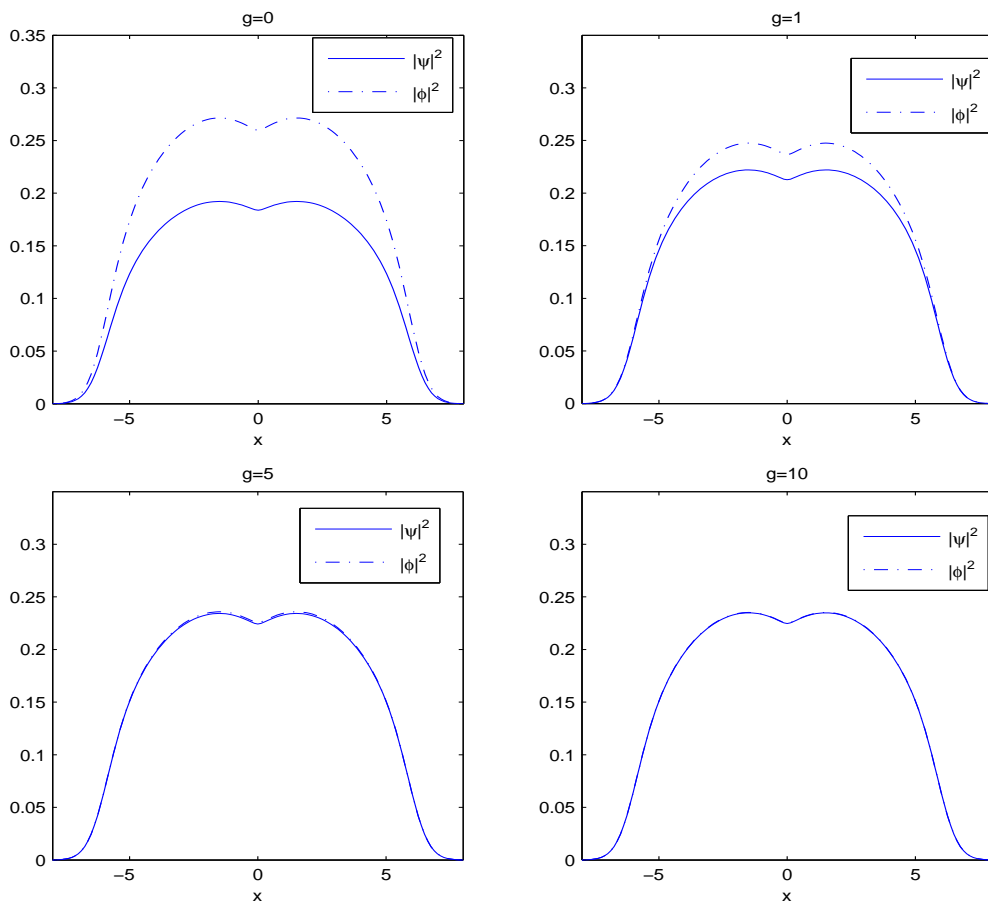
Figure 3.3: Density plots of ground states trapped in a double-well trap with different coupling strength g in **Example 3.2**.

lattice trap (i.e., $V(x) = \frac{x^2}{2} + 24\sin^2 x$) with different coupling strength g.

From Figures 3.2, 3.3 and 3.4, we can observe that as the coupling strength g grows larger, the density of two condensates become closer and closer, i.e. $|\psi|^2 \to |\phi|^2$, which suggests us that larger coupling strength g may promote the union of two independent condensates.

Our further numerical computations shown in Figure 3.5 confirm the above-mentioned observations as well, where we can see that as $g \to \infty$, $N(\psi) \to N(\phi)$ (i.e., the mass of the two condensate are almost same in the limit).

Example 3.3. In this example, we study how masses of two condensates, energy and chemical potential of ground state solutions change when coupling strength g or interaction parameter β or detuning strength δ_1 increases. In the computation, $V_1(x) = V_2(x) = \frac{1}{2}x^2$ is fixed, the other parameters are used as those in **Example 3.2** unless we
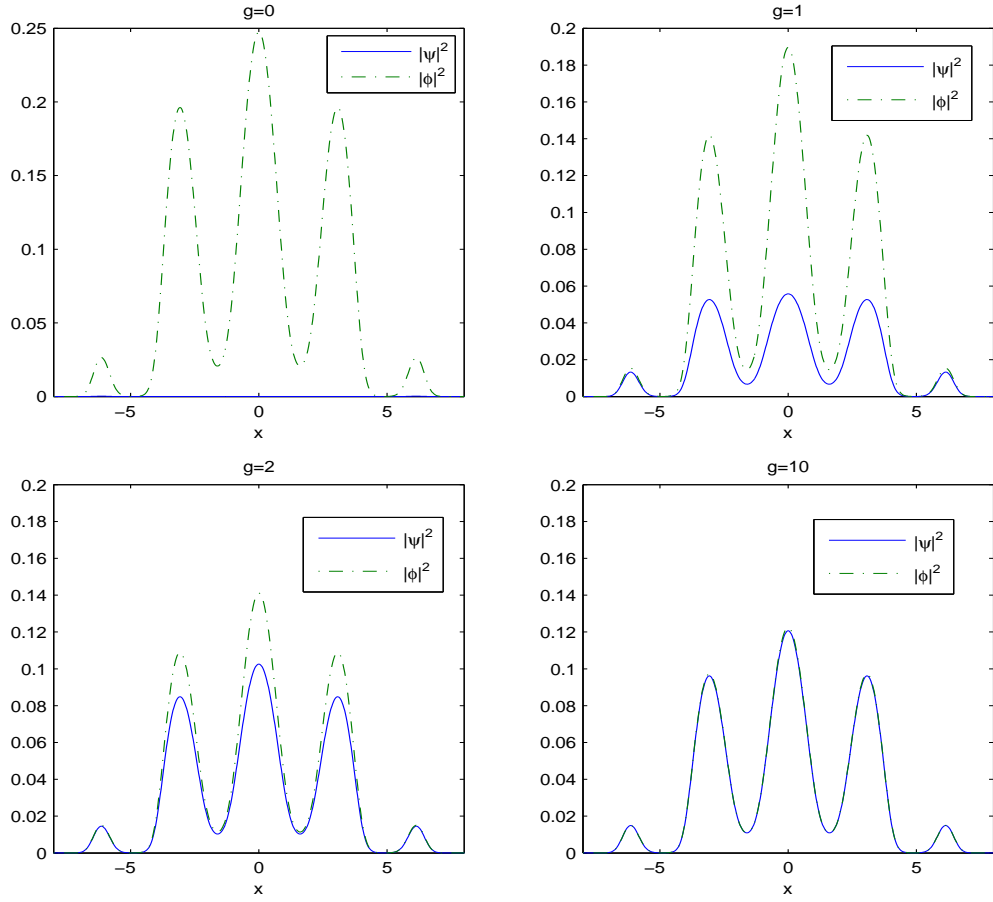
Figure 3.4: Density plots of ground states of coupling BEC trapped in an optical lattice trap with different coupling strength g in **Example 3.2**.

have specified otherwise.

Masses of two condensates and photons (i.e., $N(\psi)$ $N(\phi)$ $N(C)$), energy E and chemical potential μ of the ground state solutions for different interaction parameter β are shown in Figure 3.6. As the interaction parameter β becomes larger, it can be observed that (1) the energy E and chemical potential μ of the ground states increases (valid for $g = 0$ and $g \neq 0$); (2) masses of two condensates and photons do not change when the coupling strength $g = 0$, while masses of two condensates and photons do change when the coupling strength $g \neq 0$.

Figure 3.7 shows masses of two condensates and photons (i.e., $N(\psi)$ $N(\phi)$ $N(C)$), energy E and chemical potential μ of the ground states for different detuning strength δ_1. As δ_1 becomes larger, it can be found that (1) both the energy E and chemical potential μ of the ground states increase to a limit; (2) masses of two condensates, $N(\psi) \to 0$ and
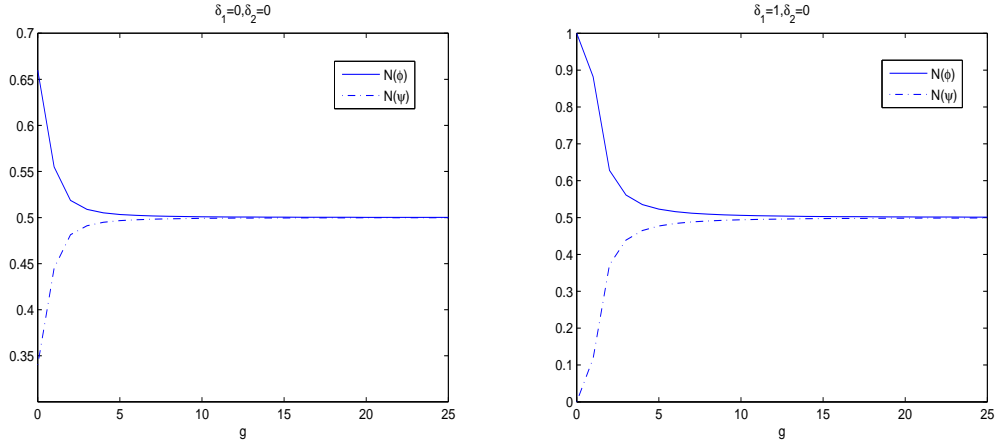
Figure 3.5: Masses of two condensates in the harmonic trap, i.e., $N(\psi), N(\phi)$ for different coupling strength g in **Example 3.2**.

$N(\phi) \to 1$, while mass of photons $N(C)$ becomes nonzero when coupling strength $g \neq 0$.

3.4.2 Ground state solutions in 2D

Example 3.4 In this example, we show that our numerical method for computing two-dimensional ground states is reliable by choosing different arbitrary initial data:

$$(1) \quad \psi(x,y,0) = \frac{\sqrt{2}}{\sqrt{3\pi}}e^{-\frac{2}{3}(x^2+y^2)}, \ \phi(x,y,0) = \frac{1}{2\sqrt{\pi}}e^{-\frac{1}{4}(x^2+y^2)}, \ C(0) = 1+i,$$

$$(2) \quad \psi(x,y,0) = \phi(x,y,0) = \frac{1}{2\sqrt{\pi}}e^{-\frac{1}{4}(x^2+y^2)}, \ C(0) = 1+2i,$$

$$(3) \quad \psi(x,y,0) = \phi(x,y,0) = \frac{\sqrt{2}}{\sqrt{3\pi}}e^{-\frac{2}{3}(x^2+y^2)}, \ \ C(0) = 3+i.$$

In the computation, we choose domain $[-8,8] \times [-8,8]$, and spacial mesh size $h_x = h_y = 1/8$, $\delta_1 = 0.5$, $\delta_2 = 0$, $\Omega = 1$, $v = 1$, $g = 1$ and $\beta_{11} : \beta_{12} : \beta_{21} : \beta_{22} = (1 : 0.94 : 0.94 : 0.97)\beta$ with $\beta = 100$.

Figure 3.8 shows us that the normalized gradient flows decay to the same ground state which has the same energy, though prepared with different data in 2D.

Example 3.5 In this example, we study the two-dimensional ground state solutions when coupling BEC are confined in different trap potentials. We choose the computation domain $[-8,8] \times [-8,8]$, and mesh size $h_x = h_y = 1/8$, $\delta_1 = \delta_2 = 0$, $\Omega = 1$, $v = 1$, $g = 1$ and $\beta_{11} : \beta_{12} : \beta_{21} : \beta_{22} = (1 : 0.94 : 0.94 : 0.97)\beta$ with $\beta = 100$.

Figure 3.6: Masses of two condensates and photons (i.e., $N(\psi)$ $N(\phi)$ $N(C)$), energy E and chemical potential μ of the ground states for different interaction parameter β.

In the numerical calculation, different trap potentials $V_1(x, y)$ and $V_2(x, y)$ have been used: the harmonic trap potentials $V_j(x, y) = \frac{1}{2}[(x - a_j)^2 + y^2]$, $(j = 1, 2)$, where a_1 and a_2 are shifts of centers of the harmonic trap potentials in x-direction; the double-well trap potential $V_1(x, y) = V_2(x, y) = \frac{1}{2}(|x| - a_3)^2 + y^2)$, where a_3 is a positive constant; the harmonic plus optical lattice trap potentials $V_1(x, y) = V_2(x, y) = \frac{1}{2}(x^2 + y^2) + p\left(\sin^2(qx) + \sin^2(qy)\right)$, where p, q are some positive constants.

Figure 3.9(a) shows us the density plots of two condensates in the harmonic traps with no shifts of centers in x-direction ($a_1 = a_2 = 0$). Figure 3.9(b) shows us the density plots of two condensates in the harmonic traps with shifts ($a_1 = -2$ and $a_2 = 2$). From these figures, we can conclude that the shifts of centers in x-direction of the harmonic trap potentials can bring about the changes of density profile of ground state solutions in the optical resonators.
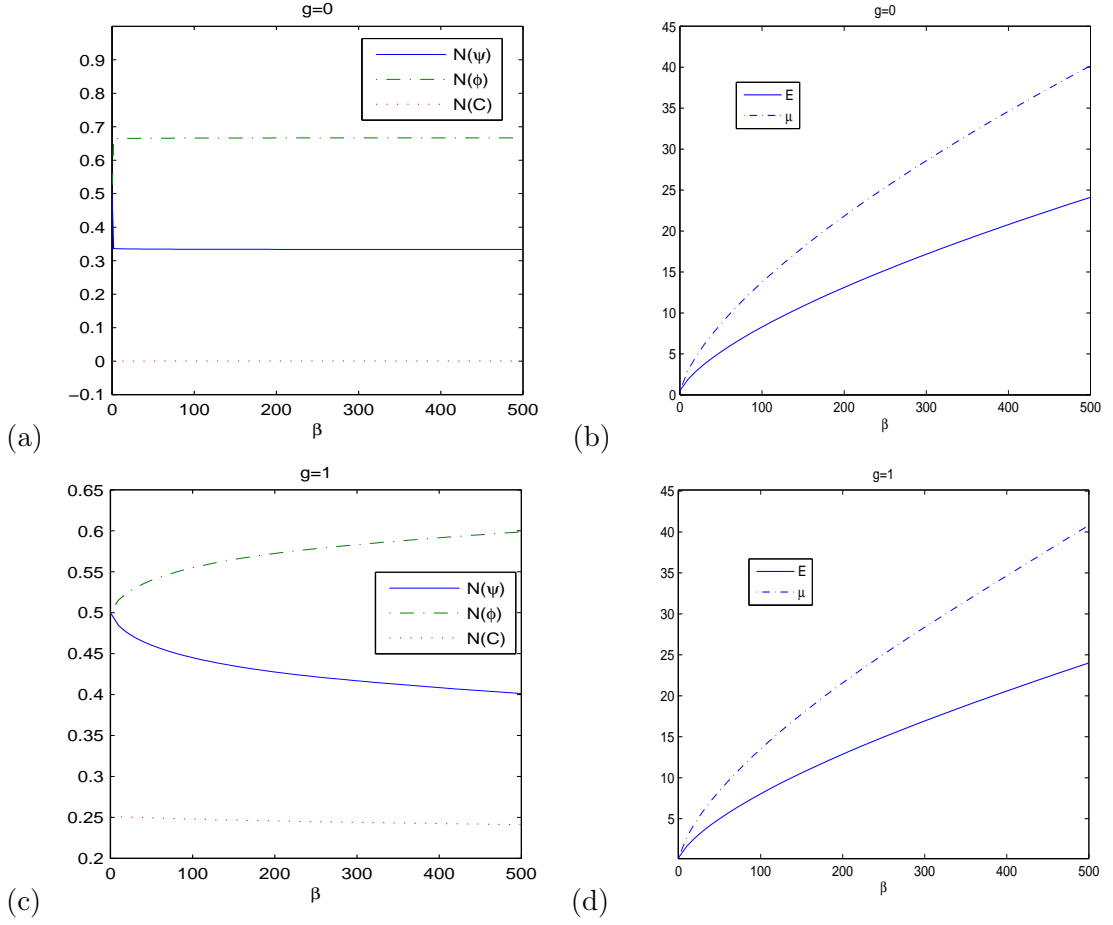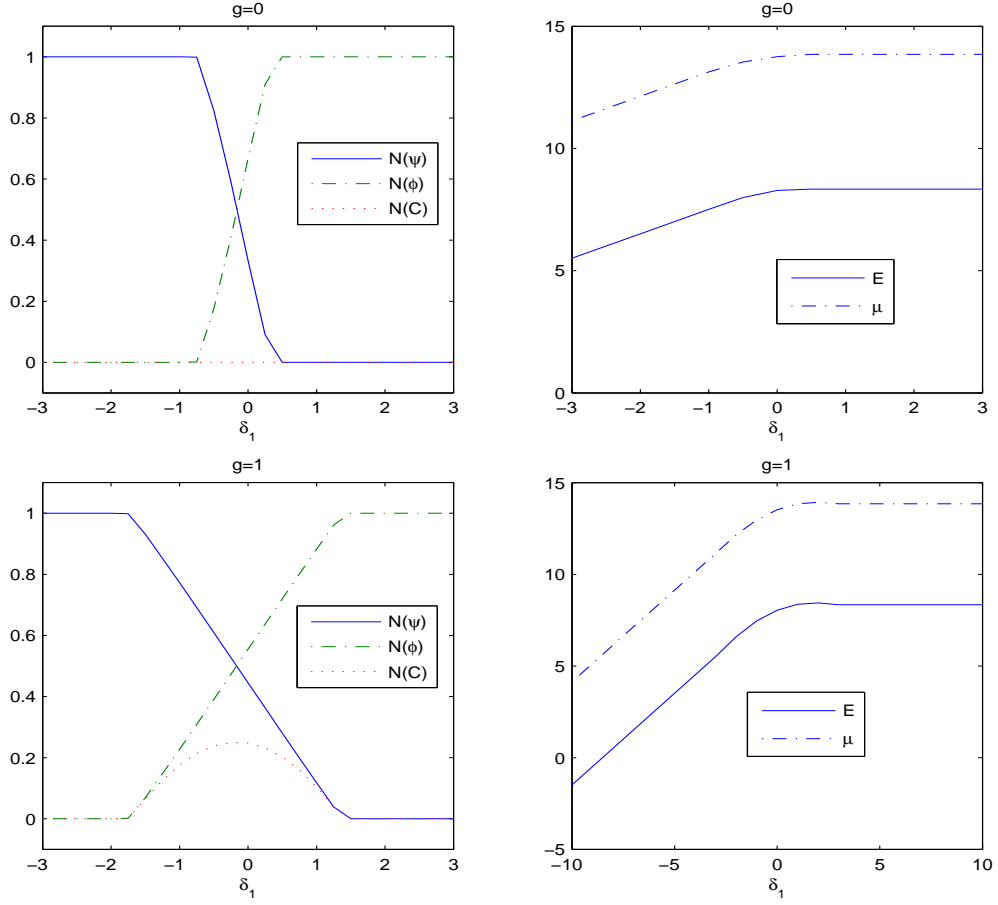
Figure 3.7: Masses of two condensates and photons (i.e., $N(\psi)$ $N(\phi)$ $N(C)$), energy E and chemical potential μ of the ground states for different detuning strength δ_1.

Figure 3.10(a) shows us the density plots of two condensates in the double well trap potentials with no shifts ($a_3 = 0$). Figure 3.10(b) shows us the density plots of two condensates in the double well trap with the shift ($a_3 = 2$). From these figures, we can conclude that the shifts of centers of the double trap potentials can bring about the changes of density profile of ground states solutions: the larger of a_3 is, the two peaks of two condensates are further away from each other.

Figure 3.11(a)(b)(c)(d) show us the density plots of two condensates in different harmonic plus optical lattice trap potentials $V_j(x,y) = \frac{1}{2}(x^2 + y^2) + p\left(\sin^2(qx) + \sin^2(qy)\right)$, j=1,2. From these figures, we can conclude that p, i.e., the magnitude of the optical lattice trap potentials can determine how many peaks of density profile of ground states solutions can have: the larger of p, the more peaks; while q, i.e., the mode of the optical lattice trap potentials can decide how deep of the density profile of ground states
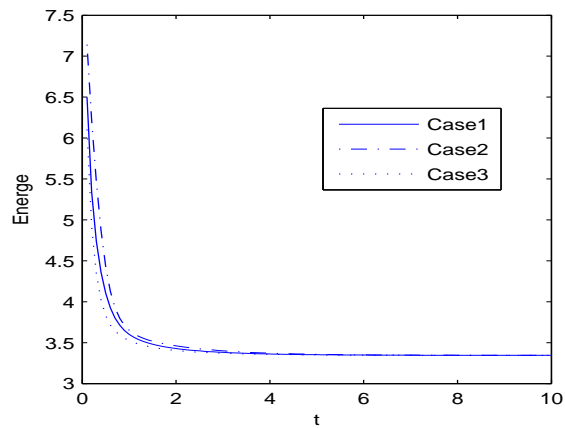
Figure 3.8: Gradient flows prepared with different initial data converge into the same steady-state solution which has the same energy in **Example 3.4**

solutions can be: the larger of q, the deeper valleys and the sharper peaks.

To sum up, we have proposed an efficient numerical method for ground state solutions of coupling BEC in optical resonators and applied it to study the various structures of ground state solutions. In Chapter 4, we investigate the dynamics of coupling BEC in optical resonators while the initial data for the dynamics are prepared with the ground state solutions obtained here.
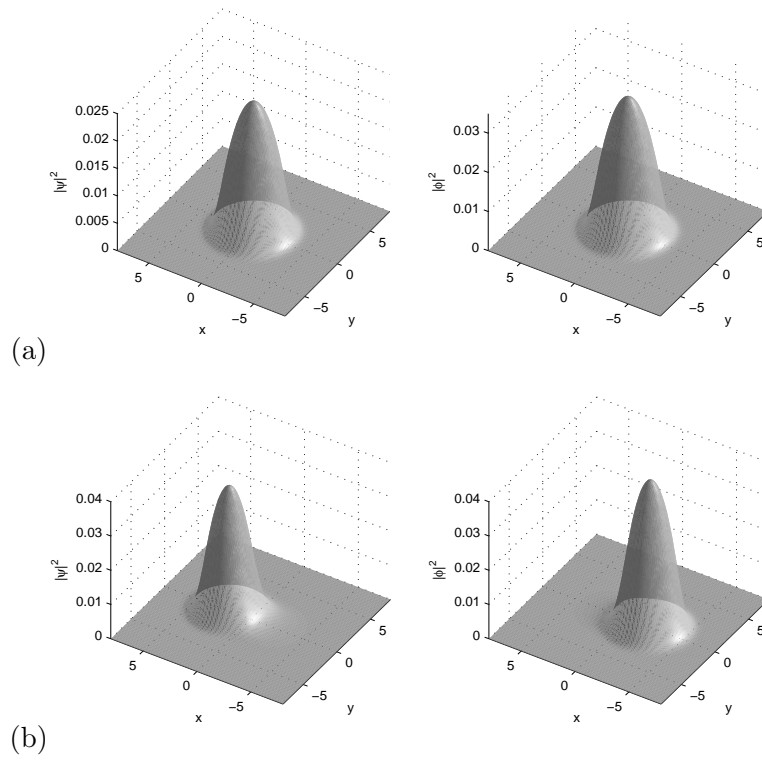
Figure 3.9: Density plots of ground states of coupling BEC in the harmonic traps (a) with no shifts of centers in x-direction, and (b) with shifts $a_1 = -2$ and $a_2 = 2$.
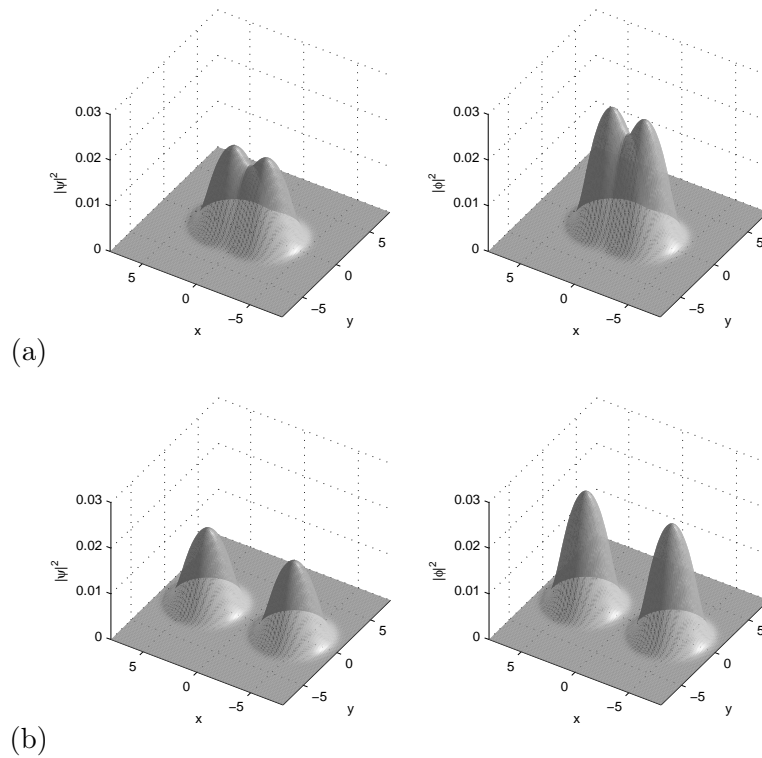
Figure 3.10: Density plots of ground states of coupling BEC in the double well trap (a) with no shift ($a_3 = 0$), and (b) with the shift $a_3 = 2$.
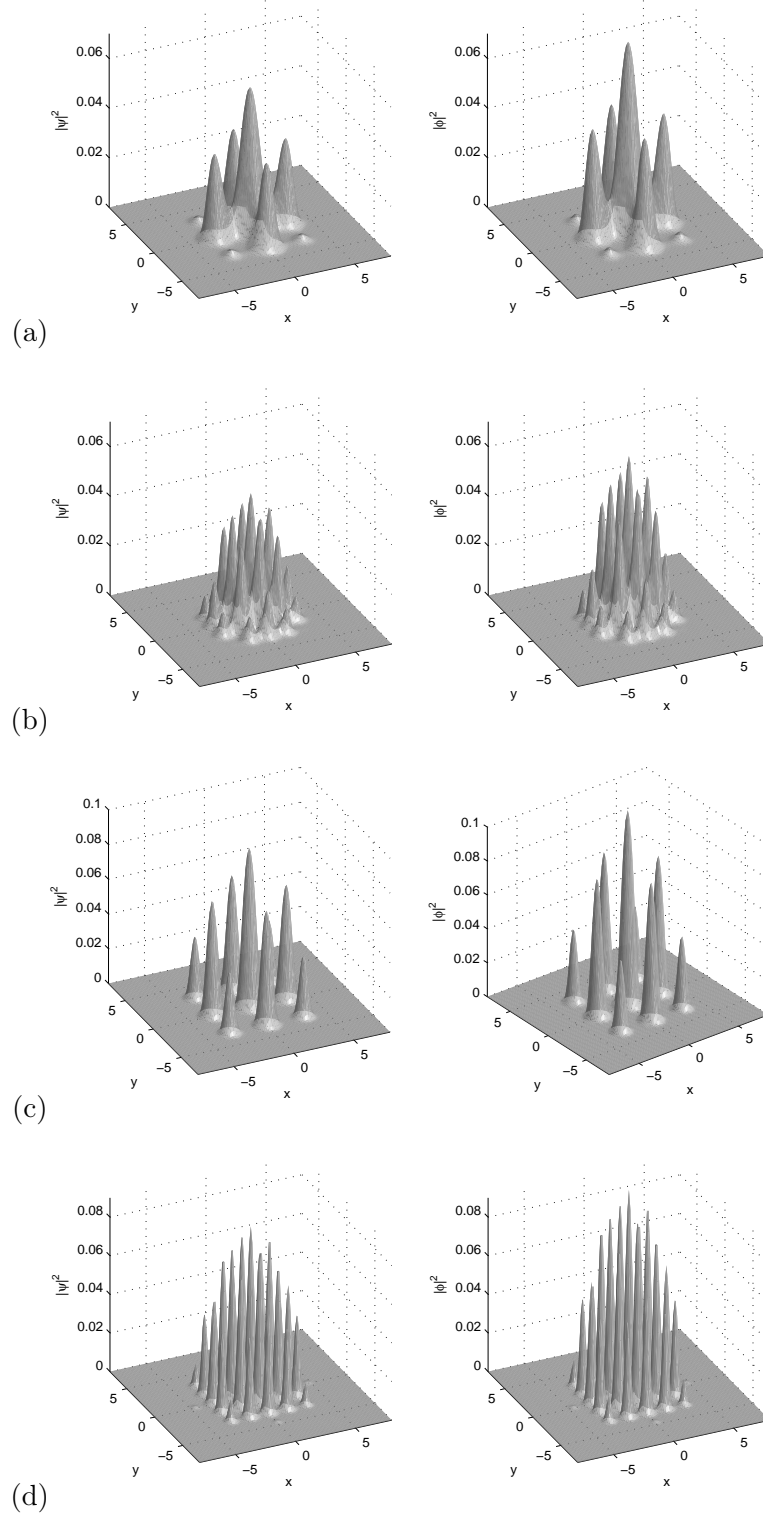
Figure 3.11: Density plots of ground states of coupling BEC in different optical lattice trap potentials $V_1(x,y) = V_2(x,y) = \frac{1}{2}(x^2 + y^2) + p(\sin^2(qx) + \sin^2(qy))$:(a) p=20,q=1; (b)p=20,q=2; (c)p=60,q=1; (d)p=60,q=2;

Chapter 4

Dynamics of coupling BEC in optical resonators

In this chapter, we study the dynamics of coupling BEC in optical resonators which are governed by the coupled equations (2.15)-(2.17).

Firstly we investigate various dynamical properties of coupling BEC in optical resonators. Secondly we propose an efficient numerical method—time-splitting Sine pseudospectral method—for the coupled equations (2.15)-(2.17). The key ideas of the method are: first using a time-splitting technique to decouple the equations (2.15)-(2.16) into nonlinear part and linear part; second adopting the Sine spectral method to discretize the linear equation while solving the nonlinear equation exactly. The integration term in the equation (2.17) may bring some difficulties when designing numerical methods without proper care. However, as we show later in numerical algorithm and numerical simulations, by carefully using the solutions obtained from time-splitting technique for the equations (2.15)-(2.16) and Taylor expansion for (2.17), we can deal with the problem quite well.

4.1 Dynamical laws

For the coupled equations (2.15)-(2.17) which describe the dynamics of coupling BEC in optical resonators, we know that they have the property of the total mass conservation,

i.e.,

$$N(\psi(\mathbf{x}, t)) + N(\phi(\mathbf{x}, t)) = 1.$$

The energy $E(\psi, \phi, C)$ related to the coupled equations (2.15)-(2.17) is also conserved. In this subsection, we consider the dynamical laws for the condensate width, which are physically interested.

4.1.1 Dynamical laws for the condensate width

First, we define the condensate width in 1D as

$$\delta_x(t) \quad = \quad \int_{\mathbb{R}} x^2 (|\psi|^2 + |\phi|^2) \, dx. \tag{4.1}$$

Second, we define the condensate width in 2D as

$$\delta(t) = \int_{\mathbb{R}^2} (x^2 + y^2)(|\psi|^2 + |\phi|^2) \, dxdy. \tag{4.2}$$

For the dynamics of the condensate width in 1D, we have the following Lemma:

Lemma 4.1.1. *Suppose $\psi(x, t)$ and $\phi(x, t)$ are the solutions of coupled equations (2.15)-(2.16) in 1D, $V_1(x) = V_2(x) = \frac{1}{2}x^2$, and $\beta_{12} = \beta_{21}$, we have*

$$\frac{d^2\delta_x(t)}{dt^2} = -2\delta_x(t) + \int_{\mathbb{R}} 2(|\partial_x\psi|^2 + |\partial_x\phi|^2) + (\beta_{11}|\psi|^4 + 2\beta_{12}|\phi|^2|\psi|^2 + \beta_{22}|\phi|^4)dx. \tag{4.3}$$

Proof: We first differentiate (4.1) with respect to t, and then we apply (2.15)-(2.16) to get

$$\begin{aligned}
\frac{d\delta_x(t)}{dt} &= \int_{\mathbb{R}} x^2 (\partial_t\psi\bar{\psi} + \partial_t\bar{\psi}\psi + \partial_t\phi\bar{\phi} + \partial_t\bar{\phi}\phi)dx \\
&= i\int_{\mathbb{R}} \frac{1}{2}x^2 \left[-\partial_{xx}\bar{\psi}\psi + \partial_{xx}\psi\bar{\psi} - \partial_{xx}\bar{\phi}\phi + \partial_{xx}\phi\bar{\phi} \right] dx. \tag{4.4}
\end{aligned}$$

By differentiating (4.4), we can get

$$
\begin{aligned}
\frac{d^2 \delta_x(t)}{dt^2} &= i \int_{\mathbb{R}} \frac{1}{2} x^2 [-\partial_t(\partial_{xx}\bar{\psi})\psi - \partial_t\psi\partial_{xx}\bar{\psi} + \partial_t(\partial_{xx}\psi)\bar{\psi} + \partial_t\bar{\psi}\partial_{xx}\psi]dx \\
&\quad + i \int_{\mathbb{R}} \frac{1}{2} x^2 [-\partial_t(\partial_{xx}\bar{\phi})\phi - \partial_t\phi\partial_{xx}\bar{\phi} + \partial_t(\partial_{xx}\phi)\bar{\phi} + \partial_t\bar{\phi}\partial_{xx}\phi]dx \\
&= F(\psi) + F(\phi),
\end{aligned}
\tag{4.5}
$$

For $F(\psi)$, we integrate by parts for each term,

$$
\begin{aligned}
F(\psi) &= \frac{1}{2}i \int_{\mathbb{R}} \left[2x\partial_t(\partial_x\bar{\psi})\psi + x^2\partial_t(\partial_x\bar{\psi})\partial_x\psi\right] + \left[2x\partial_x\bar{\psi}\partial_t\psi + x^2\partial_x\bar{\psi}\partial_t(\partial_x\psi)\right] \\
&\quad - \left[2x\partial_t(\partial_x\psi)\bar{\psi} + x^2\partial_t(\partial_x\psi)\partial_x\bar{\psi}\right] - \left[2x\partial_x\psi\partial_t\bar{\psi} + x^2\partial_x\psi\partial_t(\partial_x\bar{\psi})\right] dx \\
&= i \int_{\mathbb{R}} x\left[\partial_t(\partial_x\bar{\psi})\psi - \partial_t(\partial_x\psi)\bar{\psi}\right] + x\left[\partial_x\bar{\psi}\partial_t\psi - \partial_x\psi\partial_t\bar{\psi}\right] dx \\
&= i \int_{\mathbb{R}} \left[-\partial_t\bar{\psi}\psi - x\partial_x\psi\partial_t\bar{\psi} + \partial_t\psi\bar{\psi} + x\partial_x\bar{\psi}\partial_t\psi\right] + x\left[\partial_x\bar{\psi}\partial_t\psi - \partial_x\psi\partial_t\bar{\psi}\right] dx \\
&= \int_{\mathbb{R}} i\left[-\partial_t\bar{\psi}\psi + \partial_t\psi\bar{\psi}\right] + i\left[2x\partial_x\bar{\psi}\partial_t\psi\right] + i\left[-2x\partial_x\psi\partial_t\bar{\psi}\right] dx \\
&= A(\psi) + B(\psi) + \bar{B}(\psi),
\end{aligned}
\tag{4.6}
$$

where $A(\psi) = \int_{\mathbb{R}} i[-\partial_t\bar{\psi}\psi + \partial_t\psi\bar{\psi}]dx$, $B(\psi) = \int_{\mathbb{R}} i2x\partial_t\psi\partial_x\bar{\psi}dx$.

Similarly, for $F(\phi)$, we have

$$
\begin{aligned}
F(\phi) &= \int_{\mathbb{R}} i[-\partial_t\bar{\phi}\phi + \partial_t\phi\bar{\phi}] + i[2x\partial_x\bar{\phi}\partial_t\phi] + i[-2x\partial_x\phi\partial_t\bar{\phi}]dx \\
&= A(\phi) + B(\phi) + \bar{B}(\phi).
\end{aligned}
\tag{4.7}
$$

Next, plugging (2.15) into $A(\psi)$, we have

$$
\begin{aligned}
A(\psi) &= \int_{\mathbb{R}} \left[|\partial_x\psi|^2 + 2V_1(x)|\psi|^2 + 2(\beta_{11}|\psi|^2 + \beta_{12}|\phi|^2)|\psi|^2 + (g\bar{C}(t) + \frac{\Omega}{2})\bar{\phi}\psi \right. \\
&\quad \left. + 2\delta_1|\psi|^2 + (gC(t) + \frac{\Omega}{2})\phi\bar{\psi}\right] dx.
\end{aligned}
\tag{4.8}
$$

Similarly, we can obtain

$$
\begin{aligned}
A(\phi) &= \int_{\mathbb{R}} \left[|\partial_x\phi|^2 + 2V_2(x)|\phi|^2 + 2(\beta_{21}|\psi|^2 + \beta_{22}|\phi|^2)|\phi|^2 + (g\bar{C}(t) + \frac{\Omega}{2})\psi\bar{\phi} \right. \\
&\quad \left. + 2\delta_2|\phi|^2 + (gC(t) + \frac{\Omega}{2})\bar{\psi}\phi\right] dx.
\end{aligned}
\tag{4.9}
$$

Summing up both sides of (4.8)-(4.9), we get

$$
\begin{aligned}
A(\psi) + A(\phi) &= 2E + \int_{\mathbb{R}} (\beta_{11}|\psi|^2 + \beta_{12}|\phi|^2)|\psi|^2 + (\beta_{21}|\psi|^2 + \beta_{22}|\phi|^2)|\phi|^2 dx \\
&\quad -2v|C(t)|^2.
\end{aligned} \tag{4.10}
$$

For $B(\psi)$, we also use (2.15) and integrate by parts,

$$
\begin{aligned}
B(\psi) &= \int_{\mathbb{R}} \left\{ \left[V_1(x)\psi + (\beta_{11}|\psi|^2 + \beta_{12}|\phi|^2)\psi + (gC(t) + \frac{\Omega}{2})\phi + \delta_1\psi \right] 2x\partial_x\bar{\psi} \right. \\
&\quad \left. + (-\frac{1}{2}\partial_{xx}\psi)2x\partial_x\bar{\psi} \right\} dx \\
&= \int_{\mathbb{R}} \left[|\partial_x\psi|^2 + x\partial_x\psi\partial_{xx}\bar{\psi} - 2[V_1(x)|\psi|^2 + (\beta_{11}|\psi|^2 + \beta_{12}|\phi|^2)|\psi|^2 + (gC(t) + \right. \\
&\quad \frac{\Omega}{2})\phi\bar{\psi} + \delta_1|\psi|^2] - 2x\bar{\psi}[V_1(x) + (\beta_{11}|\psi|^2 + \beta_{12}|\phi|^2) + \delta_1]\partial_x\psi - 2x\bar{\psi}(gC(t) \\
&\quad \left. + \frac{\Omega}{2})\partial_x\phi - 2x\bar{\psi}[\partial_x V_1(x) + \partial_x(\beta_{11}|\psi|^2 + \beta_{12}|\phi|^2)]\psi \right] dx.
\end{aligned} \tag{4.11}
$$

By definition of $\bar{B}(\psi)$, (4.11) can be rewritten as

$$
\begin{aligned}
B(\psi) &= \int_{\mathbb{R}} \left[|\partial_x\psi|^2 - 2[V_1(x)|\psi|^2 + (\beta_{11}|\psi|^2 + \beta_{12}|\phi|^2)|\psi|^2 + (gC(t) + \frac{\Omega}{2})\phi\bar{\psi} \right. \\
&\quad + \delta_1|\psi|^2] - 2x\bar{\psi}[\partial_x V_1(x) + \partial_x(\beta_{11}|\psi|^2 + \beta_{12}|\phi|^2)]\psi - 2x\bar{\psi}(gC(t) + \frac{\Omega}{2})\partial_x\phi \\
&\quad \left. + 2x\bar{\phi}(g\bar{C}(t) + \frac{\Omega}{2})\partial_x\psi \right] dx - \bar{B}(\psi).
\end{aligned} \tag{4.12}
$$

Similarly, for $B(\phi)$ we can get

$$
\begin{aligned}
B(\phi) &= \int_{\mathbb{R}} \left[|\partial_x\phi|^2 - 2[V_2(x)|\phi|^2 + (\beta_{21}|\psi|^2 + \beta_{22}|\phi|^2)|\phi|^2 + (g\bar{C}(t) + \frac{\Omega}{2})\psi\bar{\phi} \right. \\
&\quad + \delta_2|\phi|^2] - 2x\bar{\phi}[\partial_x V_2(x) + \partial_x(\beta_{21}|\psi|^2 + \beta_{22}|\phi|^2)]\phi - 2x\bar{\phi}(g\bar{C}(t) + \frac{\Omega}{2})\partial_x\psi \\
&\quad \left. + 2x\bar{\psi}(gC(t) + \frac{\Omega}{2})\partial_x\phi \right] dx - \bar{B}(\phi).
\end{aligned} \tag{4.13}
$$

Combining (4.12)-(4.13), we arrive at

$$
\begin{aligned}
B(\psi) + B(\phi) \;=\; & -2E + 2v|C|^2 + \int_{\mathbb{R}} \bigg[2(|\partial_x \psi|^2 + |\partial_x \phi|^2) - [(\beta_{11}|\psi|^2 + \beta_{12}|\phi|^2)]|\psi|^2 \\
& + (\beta_{21}|\psi|^2 + \beta_{22}|\phi|^2)|\phi|^2] - 2x\bar{\phi}[\partial_x V_2(x) + \partial_x(\beta_{21}|\psi|^2 + \beta_{22}|\phi|^2)]\phi \\
& - 2x\bar{\psi}[\partial_x V_1(x) + \partial_x(\beta_{11}|\psi|^2 + \beta_{12}|\phi|^2)]\psi \bigg] dx - \bar{B}(\psi) - \bar{B}(\phi). \quad (4.14)
\end{aligned}
$$

Thus, we can get

$$
\begin{aligned}
& F(\psi) + F(\phi) \\
=\; & \int_{\mathbb{R}} \bigg[2(|\partial_x \psi|^2 + |\partial_x \phi|^2) - \Big(2x|\psi|^2 \partial_x V_1(x) + 2x|\phi|^2 \partial_x V_2(x) \Big) - \Big(2x|\psi|^2 \partial_x(\beta_{11}|\psi|^2 \\
& + \beta_{12}|\phi|^2) + 2x|\phi|^2 \partial_x(\beta_{21}|\psi|^2 + \beta_{22}|\phi|^2) \Big) \bigg] dx. \quad (4.15)
\end{aligned}
$$

Since $V_1(x) = V_2(x) = \frac{1}{2}x^2$, we have

$$
\begin{aligned}
\int_{\mathbb{R}} [-2x|\psi|^2 \partial_x V_1(x) - 2x|\phi|^2 \partial_x V_2(x)] dx \;&=\; \int_{\mathbb{R}} -2x^2(|\psi|^2 + |\phi|^2) dx \\
&=\; -2\delta_x(t). \quad (4.16)
\end{aligned}
$$

We now reduce the last term of (4.15) into a simpler form. Also using integration by parts, we gained

$$
\begin{aligned}
& \int_{\mathbb{R}} -2x|\psi|^2 \partial_x(\beta_{11}|\psi|^2 + \beta_{12}|\phi|^2) dx \\
=\; & -2\int_{\mathbb{R}} x\partial_x(\beta_{11}|\psi|^2)|\psi|^2 dx - 2\int_{\mathbb{R}} x\partial_x(\beta_{12}|\phi|^2)|\psi|^2 dx \\
=\; & -2\int_{\mathbb{R}} \beta_{11} x\partial_x[\frac{1}{2}(|\psi|^2)^2] dx + 2\int_{\mathbb{R}} \beta_{12}|\phi|^2(|\psi|^2 + x\partial_x(|\psi|^2)) dx \\
=\; & \int_{\mathbb{R}} \beta_{11}|\psi|^4 dx + 2\int_{\mathbb{R}} \beta_{12}|\phi|^2(|\psi|^2 + x\partial_x(|\psi|^2)) dx. \quad (4.17)
\end{aligned}
$$

Similarly, we have

$$
\int_{\mathbb{R}} -2x|\phi|^2 \partial_x(\beta_{21}|\psi|^2 + \beta_{22}|\phi|^2) dx = \int_{\mathbb{R}} \beta_{22}|\phi|^4 dx - 2\int_{\mathbb{R}} \beta_{21}|\phi|^2 x\partial_x(|\psi|^2) dx. \quad (4.18)
$$

Since $\beta_{12} = \beta_{21}$, we can combine (4.17)-(4.18) and eliminate $2\int \beta_{21}|\phi|^2 x\partial_x(|\psi|^2) dx$, then we finally obtain (4.3) via (4.15).

45

For the dynamics of the condensate width in 2D, we have

Lemma 4.1.2. *Suppose that $\psi(x, y, t)$ and $\phi(x, y, t)$ are the solutions of coupled equations (2.15)-(2.16) in 2D, $V_1(x, y) = V_2(x, y) = \frac{1}{2}(x^2 + y^2)$, and $\beta_{12} = \beta_{21}$, we have*

$$\frac{d^2\delta(t)}{dt^2} = -2\delta(t) + \int_{\mathbb{R}^2} \left[2(|\nabla\psi|^2 + |\nabla\phi|^2) + 2(\beta_{11}|\psi|^4 + 2\beta_{12}|\phi|^2|\psi|^2 + \beta_{22}|\phi|^4) \right] \, d\mathbf{x}.$$

The proof of the Lemma 4.1.2 can be done in a similar way as what have done for Lemma 4.1.1. Here we use Green's Formula in 2D instead of integration by parts in 1D.

From the above Lemma 4.1.2, we can easily derive the following theorem in 2D:

Theorem 4.1.3. *Suppose that $\psi(x, y, t)$ and $\phi(x, y, t)$ are the solutions of coupled equations (2.15)-(2.16) in 2D, $V_1(x, y) = V_2(x, y) = \frac{1}{2}(x^2 + y^2)$, $\beta_{12} = \beta_{21}$, and $g = \Omega = v = \delta_1 = \delta_2 = 0$, we have*

$$\frac{d^2\delta(t)}{dt^2} = -4\delta(t) + 4E(\psi, \phi, C), \tag{4.19}$$

which implies the condensate width function $\delta(t)$ is periodic with respect to time t.

4.2 Time-splitting Sine pseudospectral methods

In this section, we present time-splitting Sine pseudospectral methods for computing the dynamics of coupling BEC in the optical cavity. For simplicity of notation, the method is introduced for the case of one space dimension. Generalizations to higher dimensions are straightforward for tensor product grids and the results remain valid without modifications.

Due to the external trapping potentials $V_1(x)$ and $V_2(x)$, the absolute values of the solutions $|\psi(x, t)|$ and $|\phi(x, t)|$ will go to zero when $|x| \to \infty$. Thus, we truncate the problem (2.15)-(2.17) into a bounded domain and set homogeneous Dirichlet boundary conditions. The dynamics of coupling BEC in optical resonators is governed by the

following initial and boundary problem:

$$
\begin{aligned}
i\frac{\partial \psi(x,t)}{\partial t} &= -\frac{1}{2}\frac{\partial^2}{\partial x^2}\psi(x,t) + V_1(x)\psi(x,t) + [\beta_{11}|\psi(x,t)|^2 + \beta_{12}|\phi(x,t)|^2]\psi(x,t) \\
&\quad + (gC(t) + \frac{\Omega}{2})\phi(x,t) + \delta_1\psi(x,t), \tag{4.20}
\end{aligned}
$$

$$
\begin{aligned}
i\frac{\partial \phi(x,t)}{\partial t} &= -\frac{1}{2}\frac{\partial^2}{\partial x^2}\phi(x,t) + V_2(x)\phi(x,t) + [\beta_{21}|\psi(x,t)|^2 + \beta_{22}|\phi(x,t)|^2]\phi(x,t) \\
&\quad + (g\bar{C}(t) + \frac{\Omega}{2})\psi(x,t) + \delta_2\phi(x,t), \tag{4.21}
\end{aligned}
$$

$$
i\frac{\partial C(t)}{\partial t} = \int_a^b g\bar{\phi}(x,t)\psi(x,t)dx + (v - \frac{i\kappa}{2})C(t), \quad x \in \Omega_x, \tag{4.22}
$$

with given initial data

$$
\psi(x,0) = \psi^0(x), \ \phi(x,0) = \phi^0(x), \ C(0) = C^0, \quad x \in \Omega_x, \tag{4.23}
$$

and boundary conditions

$$
\psi(x,t) = 0, \ \phi(x,t) = 0, \quad x \in \partial\Omega_x, \ t \geq 0. \tag{4.24}
$$

Here κ, which puts the coupling BEC into a dissipative ring cavity [27], is the decay rate of the coupling strength g.

In the computation, we choose $\Omega_x = [a,b]$ with $|a|$, $|b|$ sufficiently large and define $\triangle t \ (> 0)$ as the time step. We choose the spatial mesh sizes $h_x = \triangle x > 0$ with $h_x = (b-a)/M$ (M is an even positive integers). We define grid points and time steps by $x_j := a + j\,h_x, \quad j = 0, 1, \cdots, M; \quad t_n := n\,\triangle t, \quad n = 0, 1, 2, \cdots$. Let ψ_j^n, ϕ_j^n and C^n be the numerical approximation of $\psi(x_j, t_n)$, $\phi(x_j, t_n)$ and $C(t_n)$, respectively.

From time $t = t_n = n\triangle t$ to $t = t_{n+1} = (n+1)\triangle t$, for n = 1, 2, 3 ..., the problem (4.20)-(4.21) can be solved in three splitting steps. One first solves

$$
i\frac{\partial \psi(x,t)}{\partial t} = -\frac{1}{2}\frac{\partial^2}{\partial x^2}\psi(x,t), \tag{4.25}
$$

$$
i\frac{\partial \phi(x,t)}{\partial t} = -\frac{1}{2}\frac{\partial^2}{\partial x^2}\phi(x,t), \tag{4.26}
$$

for the time step of length $\triangle t$, followed by solving

$$i\frac{\partial\psi(x,t)}{\partial t} = [V_1(x) + \delta_1 + \beta_{11}|\psi(x,t)|^2 + \beta_{12}|\phi(x,t)|^2]\psi(x,t), \qquad (4.27)$$

$$i\frac{\partial\phi(x,t)}{\partial t} = [V_2(x) + \delta_2 + \beta_{21}|\psi(x,t)|^2 + \beta_{22}|\phi(x,t)|^2]\phi(x,t), \qquad (4.28)$$

for the same time step, and then by solving

$$i\frac{\partial\psi(x,t)}{\partial t} = (gC + \frac{\Omega}{2})\phi(x,t), \qquad (4.29)$$

$$i\frac{\partial\phi(x,t)}{\partial t} = (g\bar{C} + \frac{\Omega}{2})\psi(x,t), \qquad (4.30)$$

for the same time step.

We can solve equations (4.25)-(4.26) with the following Sine pseudospectral method. Suppose that

$$\psi(x_j,t) = \sum_{l=1}^{M-1} \hat{\psi}_l(t)\sin(\mu_l(x_j - a)), \quad \phi(x_j,t) = \sum_{l=1}^{M-1} \hat{\phi}_l(t)\sin(\mu_l(x_j - a)), \qquad (4.31)$$

where $\mu_l = \frac{\pi l}{b-a}$ and

$$\hat{\psi}_l(t) = \frac{2}{M}\sum_{j=1}^{M-1} \psi(x_j,t)\sin(\mu_l(x_j - a)), \quad \hat{\phi}_l(t) = \frac{2}{M}\sum_{j=1}^{M-1} \phi(x_j,t)\sin(\mu_l(x_j - a)). \,(4.32)$$

Plugging (4.31) into equations (4.25)-(4.26), we have

$$i\frac{d\hat{\psi}_l}{dt} = \frac{\mu_l^2\hat{\psi}_l}{2}, \qquad (4.33)$$

$$i\frac{d\hat{\phi}_l}{dt} = \frac{\mu_l^2\hat{\phi}_l}{2}, \qquad (4.34)$$

which can be solved exactly by

$$\hat{\psi}_l(t) = e^{-\frac{i}{2}\mu_l^2(t-t_n)}\hat{\psi}_l^n, \qquad (4.35)$$

$$\hat{\phi}_l(t) = e^{-\frac{i}{2}\mu_l^2(t-t_n)}\hat{\phi}_l^n. \qquad (4.36)$$

Thus for equations (4.25)-(4.26), we can solve them through

$$\psi(x_j, t) = \sum_{l=1}^{M-1} e^{-\frac{i}{2}\mu_l^2(t-t_n)} \hat{\psi}_l^n \sin(\mu_l(x_j - a)), \tag{4.37}$$

$$\phi(x_j, t) = \sum_{l=1}^{M-1} e^{-\frac{i}{2}\mu_l^2(t-t_n)} \hat{\phi}_l^n \sin(\mu_l(x_j - a)), \tag{4.38}$$

for any $t \in [t_n, t_{n+1}]$

For equations (4.27)-(4.28), we can solve them exactly and obtain for any $t \in [t_n, t_{n+1}]$

$$\psi(x_j, t) = e^{-i[V_1(x_j)+\delta_1+\beta_{11}|\psi(x_j,t_n)|^2+\beta_{12}|\phi(x_j,t_n)|^2](t-t_n)} \psi(x_j, t_n), \tag{4.39}$$

$$\phi(x_j, t) = e^{-i[V_2(x_j)+\delta_2+\beta_{21}|\psi(x_j,t_n)|^2+\beta_{22}|\phi(x_j,t_n)|^2](t-t_n)} \phi(x_j, t_n). \tag{4.40}$$

To solve the equations (4.29)-(4.30), we rewrite it as

$$i\vec{\xi}_t = B(t)\vec{\xi}, \tag{4.41}$$

where $\vec{\xi} = \begin{pmatrix} \psi \\ \phi \end{pmatrix}$, $B(t) = \begin{pmatrix} 0 & S(t) \\ \bar{S}(t) & 0 \end{pmatrix}$, with $S(t) = gC(t) + \frac{\Omega}{2}$.

Solving the ODE system (4.41) by means of the trapezoidal rule gives us

$$
\begin{aligned}
\xi^{n+1} &= e^{-i\int_{t_n}^{t_{n+1}} B(s)ds} \xi^n \\
&= e^{-\frac{i}{2}[B(t_n)+B(t_{n+1})]\triangle t} \xi^n.
\end{aligned} \tag{4.42}
$$

To facilitate our computation of the above system, we denote

$$
\begin{aligned}
B_{n+\frac{1}{2}} &= B(t_n) + B(t_{n+1}) \\
&= \begin{pmatrix} 0 & S_{n+\frac{1}{2}} \\ \bar{S}_{n+\frac{1}{2}} & 0 \end{pmatrix},
\end{aligned} \tag{4.43}
$$

where $S_{n+\frac{1}{2}} = S(t_n) + S(t_{n+1})$. Since the matrix $B_{n+\frac{1}{2}}$ is a complex Hermitian matrix, we can factorize it into the following formulation

$$B_{n+\frac{1}{2}} = P_{n+\frac{1}{2}} D_{n+\frac{1}{2}} P_{n+\frac{1}{2}}^{-1}, \tag{4.44}$$

49

where $D_{n+\frac{1}{2}}$ is a 2×2 diagonal matrix which is composed by the eigenvalues of $B_{n+\frac{1}{2}}$, and $P_{n+\frac{1}{2}}$ is a matrix which is composed by two independent eigenvectors of $B_{n+\frac{1}{2}}$.

We first compute the eigenvalues of matrix $B_{n+\frac{1}{2}}$. First we let

$$|\lambda I - B_{n+\frac{1}{2}}| = 0, \tag{4.45}$$

thus we can get its two eigenvalues $\lambda_1 = |S_{n+\frac{1}{2}}|$ and $\lambda_2 = -|S_{n+\frac{1}{2}}|$.

Next we compute the corresponding eigenvectors of $\lambda_1 = |S_{n+\frac{1}{2}}|$. By solving the following equations

$$(\lambda_1 I - B_{n+\frac{1}{2}})\overrightarrow{v_1} = 0, \tag{4.46}$$

where $\overrightarrow{v_1} = \begin{pmatrix} y_1 \\ y_2 \end{pmatrix}$, i.e,

$$\begin{pmatrix} |S_{n+\frac{1}{2}}| & -S_{n+\frac{1}{2}} \\ -\bar{S}_{n+\frac{1}{2}} & |S_{n+\frac{1}{2}}| \end{pmatrix} \begin{pmatrix} y_1 \\ y_2 \end{pmatrix} = 0, \tag{4.47}$$

one easily gets $\overrightarrow{v_1} = \begin{pmatrix} \frac{S_{n+\frac{1}{2}}}{\sqrt{2}|S_{n+\frac{1}{2}}|} \\ \frac{1}{\sqrt{2}} \end{pmatrix}$.

Similarly, by solving the equations

$$(\lambda_2 I - B_{n+\frac{1}{2}})\overrightarrow{v_2} = 0, \tag{4.48}$$

we get one eigenvector $\overrightarrow{v_2} = \begin{pmatrix} \frac{S_{n+\frac{1}{2}}}{\sqrt{2}|S_{n+\frac{1}{2}}|} \\ -\frac{1}{\sqrt{2}} \end{pmatrix}$ of λ_2.

Then $P_{n+\frac{1}{2}} = \begin{pmatrix} \frac{S_{n+\frac{1}{2}}}{\sqrt{2}|S_{n+\frac{1}{2}}|} & \frac{S_{n+\frac{1}{2}}}{\sqrt{2}|S_{n+\frac{1}{2}}|} \\ \frac{1}{\sqrt{2}} & -\frac{1}{\sqrt{2}} \end{pmatrix}$ and $D_{n+\frac{1}{2}} = \begin{pmatrix} |S_{n+\frac{1}{2}}| & 0 \\ 0 & -|S_{n+\frac{1}{2}}| \end{pmatrix}$.

Because of the factorization (4.44), we can rewrite (4.42) as

$$
\begin{aligned}
\xi^{n+1} &= P_{n+1/2} e^{-\frac{i}{2} D_{n+\frac{1}{2}} \triangle t} P_{n+1/2}^{-1} \xi^n \\
&= \begin{pmatrix} \cos(\frac{\triangle t}{2} |S_{n+\frac{1}{2}}|) & -i \frac{S_{n+\frac{1}{2}}}{|S_{n+\frac{1}{2}}|} \sin(\frac{\triangle t}{2} |S_{n+\frac{1}{2}}|) \\ -i \frac{\bar{S}_{n+\frac{1}{2}}}{|S_{n+\frac{1}{2}}|} \sin(\frac{\triangle t}{2} |S_{n+\frac{1}{2}}|) & \cos(\frac{\triangle t}{2} |S_{n+\frac{1}{2}}|) \end{pmatrix} \xi^n.
\end{aligned}
\tag{4.49}
$$

That is, we can solve equations (4.29)-(4.30) through

$$
\psi(x_j, t_{n+1}) = \cos(\frac{\triangle t}{2} |S_{n+\frac{1}{2}}|) \psi(x_j, t_n) - i \frac{S_{n+\frac{1}{2}}}{|S_{n+\frac{1}{2}}|} \sin(\frac{\triangle t}{2} |S_{n+\frac{1}{2}}|) \phi(x_j, t_n), \tag{4.50}
$$

$$
\phi(x_j, t_{n+1}) = -i \frac{\bar{S}_{n+\frac{1}{2}}}{|S_{n+\frac{1}{2}}|} \sin(\frac{\triangle t}{2} |S_{n+\frac{1}{2}}|) \psi(x_j, t_n) + \cos(\frac{\triangle t}{2} |S_{n+\frac{1}{2}}|) \phi(x_j, t_n). \tag{4.51}
$$

To solve the equation (4.22), we should note that there is an integral term in this ordinary differential equation. However, we can get an efficient solver through the following integration factor method.

To do this, we first rewrite the equation (4.22) as

$$
C_t + (iv + \frac{\kappa}{2}) C(t) = -i \int_{\mathbb{R}} g \bar{\phi} \psi dx, \tag{4.52}
$$

then multiply its both sides by $e^{(iv+\frac{\kappa}{2})(t-t_n)}$, we get

$$
\frac{d\left[e^{(iv+\frac{\kappa}{2})(t-t_n)} C(t) \right]}{dt} = -i e^{(iv+\frac{\kappa}{2})(t-t_n)} \int_{\mathbb{R}} g \bar{\phi} \psi dx. \tag{4.53}
$$

Integrating the equation (4.53) from t_n to t_{n+1} on both sides and solving it, we have

$$
\begin{aligned}
& e^{(iv+\frac{\kappa}{2})\triangle t} C(t_{n+1}) - C(t_n) \\
&= \int_{t_n}^{t_{n+1}} -i e^{(iv+\frac{\kappa}{2})(t-t_n)} \int_{\mathbb{R}} g \bar{\phi} \psi dx dt, \\
&= i \frac{\Delta t}{2} \left[e^{(iv+\frac{\kappa}{2})\Delta t} \left(- \int_{\mathbb{R}} g \bar{\phi}(x, t_{n+1}) \psi(x, t_{n+1}) dx \right) - \int_{\mathbb{R}} g \bar{\phi}(x, t_n) \psi(x, t_n) dx \right].
\end{aligned}
$$

Thus, we obtain

$$C(t_{n+1}) = e^{-(iv+\frac{\kappa}{2})\triangle t} \left[C(t_n) - i\frac{\triangle t}{2} \int_{\mathbb{R}} g\bar{\phi}(x,t_n)\psi(x,t_n)dx \right]$$
$$-i\frac{\triangle t}{2} \int_{\mathbb{R}} g\bar{\phi}(x,t_{n+1})\psi(x,t_{n+1})dx. \tag{4.54}$$

The righthand side of the above equation includes unknown term $\psi(x,t_{n+1})$ and $\bar{\phi}(x,t_{n+1})$. In the following, we estimate them by the Taylor expansion at t_n to the first order and get

$$i\frac{\triangle t}{2} \int_{\mathbb{R}} g\bar{\phi}(x,t_{n+1})\psi(x,t_{n+1})dx$$
$$= i\frac{\triangle t}{2} \int_{\mathbb{R}} g\bar{\phi}(x,t_n)\psi(x,t_n)dx + i\frac{(\triangle t)^2}{2}\frac{\partial}{\partial t} \int_{\mathbb{R}} g\bar{\phi}(x,t_n)\psi(x,t_n)dx. \tag{4.55}$$

Since $i\bar{\phi}_t, \ i\psi_t$ could be calculated by equations (4.20) and (4.21), we get

$$i\frac{\partial}{\partial t} \int_{\mathbb{R}} \bar{\phi}\psi dx = i\int_{\mathbb{R}} \partial_t\bar{\phi}\psi + \bar{\phi}\partial_t\psi dx,$$
$$= -\int_{\mathbb{R}} \psi \left[-\frac{1}{2}\partial_{xx}\bar{\phi} + V_2\bar{\phi} + (\beta_{21}|\psi|^2 + \beta_{22}|\phi|^2)\bar{\phi} + (gC(t) + \frac{\Omega}{2})\bar{\psi} + \delta_2\bar{\phi} \right]$$
$$+ \bar{\phi} \left[-\frac{1}{2}\partial_{xx}\psi + V_1\psi + (\beta_{11}|\psi|^2 + \beta_{12}|\phi|^2)\psi + (gC(t) + \frac{\Omega}{2})\phi + \delta_1\psi \right] dx,$$
$$= -\int_{\mathbb{R}} \left[\psi\bar{\phi}[V_2 - V_1 + (\beta_{12} - \beta_{11})|\psi|^2 + (\beta_{22} - \beta_{21})|\phi|^2 + \delta_2 - \delta_1] \right.$$
$$\left. + (gC(t) + \frac{\Omega}{2})(|\psi|^2 - |\phi|^2) \right] dx$$
$$:= \mathcal{J}(t). \tag{4.56}$$

Substituting (4.56) into (4.54), finally we obtain the solution of the equation (4.22)

$$C(t_{n+1}) = e^{-(iv+\frac{\kappa}{2})\triangle t}[C(t_n) - \mathcal{L}(t_n)] - \mathcal{L}(t_n) - \frac{(\triangle t)^2}{2}g\mathcal{J}(t_n), \tag{4.57}$$

where $\mathcal{L}(t_n) := i\frac{\triangle t}{2} \int g\bar{\phi}(x,t_n)\psi(x,t_n)dx.$

When we combine (4.25)-(4.26), (4.27)-(4.28) and (4.29)-(4.30) by the first-order time-splitting method, we get the following three-step splitting method, i.e., from time $t = t_n$ to $t = t_{n+1}$, (i) evolve (4.25)-(4.26) for the time step $\triangle t$ with the initial data ψ^n, ϕ^n, C^n given at $t = t_n$; (ii) evolve (4.27)-(4.28) for the time step $\triangle t$ with the new data

obtained in (i); (iii) evolve (4.29)-(4.30) for the time step $\triangle t$ with the new data obtained in (ii) to get ψ^{n+1}, ϕ^{n+1}; solve the equation (4.22) from C^n and obtain C^{n+1}. The detailed algorithm of the first-order time-splitting Sine pseudospectral method (TSSP1) is as follows:

$$C^{n+1} = e^{-(iv+\frac{\kappa}{2})\triangle t}\left[C(t_n) - \mathcal{L}(t_n)\right] - \mathcal{L}(t_n) - \frac{(\triangle t)^2}{2}g\mathcal{J}(t_n),$$

$$(i) \quad \psi_j^* = \sum_{l=1}^{M-1} e^{-\frac{i}{2}\mu_l^2\triangle t}\hat{\psi}_l^n \sin(\mu_l(x_j - a)), \quad j = 0, 1, \cdots, M,$$

$$\phi_j^* = \sum_{l=1}^{M-1} e^{-\frac{i}{2}\mu_l^2\triangle t}\hat{\phi}_l^n \sin(\mu_l(x_j - a)),$$

$$(ii) \quad \psi_j^{**} = e^{-i[V_1(x_j)+\delta_1+\beta_{11}|\psi_j^*|^2+\beta_{12}|\phi_j^*|^2]\triangle t}\psi_j^*,$$

$$\phi_j^{**} = e^{-i[V_2(x_j)+\delta_2+\beta_{21}|\psi_j^*|^2+\beta_{22}|\phi_j^*|^2]\triangle t}\phi_j^*,$$

$$(iii) \quad \psi_j^{n+1} = \cos(\frac{\triangle t}{2}|S_{n+\frac{1}{2}}|)\psi_j^{**} - i\frac{S_{n+\frac{1}{2}}}{|S_{n+\frac{1}{2}}|}\sin(\frac{\triangle t}{2}|S_{n+\frac{1}{2}}|)\phi_j^{**},$$

$$\phi_j^{n+1} = -i\frac{\bar{S}_{n+\frac{1}{2}}}{|S_{n+\frac{1}{2}}|}\sin(\frac{\triangle t}{2}|S_{n+\frac{1}{2}}|)\psi_j^{**} + \cos(\frac{\triangle t}{2}|S_{n+\frac{1}{2}}|)\phi_j^{**}, \qquad (4.58)$$

where $S_{n+\frac{1}{2}} = g\left(C^n + C^{n+1}\right) + \Omega$.

When we combine (4.25)-(4.26), ((4.27)-(4.28)) and (4.29-(4.30) by the second-order time-splitting method [7], we may get the following five-step splitting method, i.e., from time $t = t_n$ to $t = t_{n+1}$, (i) evolve (4.25)-(4.26) for the time step $\triangle t/2$ with the initial data ψ^n, ϕ^n, C^n given at $t = t_n$; (ii) evolve (4.27)-(4.28) for the time step $\triangle t/2$ with the new data obtained in (i); (iii) evolve (4.29)-(4.30) for the time step $\triangle t$ with the new data obtained in (ii); (iv) evolve (4.27)-(4.28) for the time step $\triangle t/2$ with the new data obtained in (iii); v) evolve (4.25)-(4.26) for the time step $\triangle t/2$ with with the new data obtained in (iv) to get ψ^{n+1}, ϕ^{n+1}; solve the equation (4.22) from C^n and obtain C^{n+1}. The detailed algorithm of the second-order time-splitting Sine pseudospectral method

(TSSP2) is as follows:

$$C^{n+1} = e^{-(iv+\frac{\kappa}{2})\triangle t} \left[C(t_n) - \mathcal{L}(t_n) \right] - \mathcal{L}(t_n) - \frac{(\triangle t)^2}{2} g \mathcal{J}(t_n),$$

$$(i) \quad \psi_j^{(1)} = \sum_{l=1}^{M-1} e^{-\frac{i}{4}\mu_l^2 \triangle t} \hat{\psi}_l^n \sin(\mu_l(x_j - a)),$$

$$\phi_j^{(1)} = \sum_{l=1}^{M-1} e^{-\frac{i}{4}\mu_l^2 \triangle t} \hat{\phi}_l^n \sin(\mu_l(x_j - a)),$$

$$(ii) \quad \psi_j^{(2)} = e^{-i[V_1(x_j)+\delta_1+\beta_{11}|\psi_j^{(1)}|^2+\beta_{12}|\phi_j^{(1)}|^2]\triangle t/2} \psi_j^{(1)}, \quad j = 0, 1, \cdots, M,$$

$$\phi_j^{(2)} = e^{-i[V_2(x_j)+\delta_2+\beta_{21}|\psi_j^{(1)}|^2+\beta_{22}|\phi_j^{(1)}|^2]\triangle t/2} \phi_j^{(1)},$$

$$(iii) \quad \psi_j^{(3)} = \cos(\frac{\triangle t}{2}|S_{n+\frac{1}{2}}|)\psi_j^{(2)} - i\frac{S_{n+\frac{1}{2}}}{|S_{n+\frac{1}{2}}|}\sin(\frac{\triangle t}{2}|S_{n+\frac{1}{2}}|)\phi_j^{(2)},$$

$$\phi_j^{(3)} = -i\frac{\bar{S}_{n+\frac{1}{2}}}{|S_{n+\frac{1}{2}}|}\sin(\frac{\triangle t}{2}|S_{n+\frac{1}{2}}|)\psi_j^{(2)} + \cos(\frac{\triangle t}{2}|S_{n+\frac{1}{2}}|)\phi_j^{(2)},$$

$$(iv) \quad \psi_j^{(4)} = e^{-i[V_1(x_j)+\delta_1+\beta_{11}|\psi_j^{(3)}|^2+\beta_{12}|\phi_j^{(3)}|^2]\triangle t/2} \psi_j^{(3)},$$

$$\phi_j^{(4)} = e^{-i[V_2(x_j)+\delta_2+\beta_{21}|\psi_j^{(3)}|^2+\beta_{22}|\phi_j^{(3)}|^2]\triangle t/2} \phi_j^{(3)},$$

$$(v) \quad \psi_j^{n+1} = \sum_{l=1}^{M-1} e^{-\frac{i}{4}\mu_l^2 \triangle t} \hat{\psi}_l^{(4)} \sin(\mu_l(x_j - a)),$$

$$\phi_j^{n+1} = \sum_{l=1}^{M-1} e^{-\frac{i}{4}\mu_l^2 \triangle t} \hat{\phi}_l^{(4)} \sin(\mu_l(x_j - a)), \tag{4.59}$$

where $S_{n+\frac{1}{2}} = g\left(C^n + C^{n+1}\right) + \Omega$.

In the numerical simulations presented later, we will test the space accuracy and time accuracy of TSSP1 and TSSP2, respectively.

4.3 Accuracy tests

In this section, firstly, we test the numerical accuracy of two proposed time-splitting schemes TSSP1 (4.58) and TSSP2 (4.59). Second, we test some dynamics properties previously mentioned.

4.3.1 Accuracy tests in 1D

To begin with, we compute numerical solutions with a very fine mesh $h = \frac{1}{32}$ and a very small time step $\Delta t = 0.0001$, which are denoted as the 'exact' solutions, ψ^e, ϕ^e. In

Δt	$\frac{1}{20}$	$\frac{1}{40}$	$\frac{1}{80}$
$\parallel \psi^e - \psi_{\Delta x, \Delta t} \parallel_2$	1.043e-02	5.038e-03	2.475e-03
$\parallel \phi^e - \phi_{\Delta x, \Delta t} \parallel_2$	4.268e-02	2.134e-02	1.064e-02

Table 4.1: Temporal error analysis for TSSP1 in 1D: errors at t=5.0 with $\Delta x = \frac{1}{32}$

Δt	$\frac{1}{20}$	$\frac{1}{40}$	$\frac{1}{80}$
$\parallel \psi^e - \psi_{\Delta x, \Delta t} \parallel_2$	2.064e-03	5.156e-04	1.289e-04
$\parallel \phi^e - \phi_{\Delta x, \Delta t} \parallel_2$	2.153e-03	5.361e-04	1.338e-04

Table 4.2: Temporal error analysis for TSSP2 in 1D: errors at t=5.0 with $\Delta x = \frac{1}{32}$

addition, for brevity, we denote $\psi_{\Delta x, \Delta t}$, $\phi_{\Delta x, \Delta t}$ as our numerical solutions with mesh size Δx and time step Δt.

We solve the problem in the interval $[-30, 30]$, which is large enough to avoid exceeding the boundary. We take the following parameters $V(x) = \frac{x^2}{2}$, $\delta_1 = 1$, $\delta_2 = 0$, $\Omega = 1$, $g = 1$, $v = 1$, $\kappa = 1$ and $\beta_{11} : \beta_{12} : \beta_{21} : \beta_{22} = \beta(1 : 0.94 : 0.94 : 0.97)$ with $\beta = 10$. And terminal time is at t=5. Without loss of generality, we choose a Gaussian function and a complex number as initial values, which are

$$\psi(x,0) = \phi(x,0) = \frac{1}{\sqrt{2}\pi^{\frac{1}{4}}} e^{-\frac{x^2}{2}}, \ C(0) = 1 + i.$$

For time accuracy tests, we fix a fine mesh size $\Delta x = \frac{1}{32}$. Table 4.1 and Table 4.2 show discretization errors in time for TSSP1 (4.58) and TSSP2 (4.59) in 1D. For spatial accuracy tests, we choose a very small time step $\Delta t = 0.0001$. Table 4.3 shows the results of spatial discretization errors of TSSP1 in 1D. Table 4.4 shows the results of spatial discretization errors of TSSP2 in 1D.

From Tables 4.1-4.4, we can conclude for 1D that (i) Scheme TSSP1 (4.58) is of spectral accuracy in space and first order in time; (ii) Scheme TSSP2 (4.59) is of spectral accuracy in space and second order in time; (iii) Scheme TSSP1 (4.58) and Scheme TSSP2 (4.59) have similar spatial accuracy.

Δx	$\frac{1}{2}$	$\frac{1}{4}$	$\frac{1}{8}$
$\parallel \psi^e - \psi_{\Delta x, \Delta t} \parallel_2$	1.507e-02	2.720e-06	1.503e-11
$\parallel \phi^e - \phi_{\Delta x, \Delta t} \parallel_2$	1.687e-02	3.199e-06	1.681e-11

Table 4.3: Spatial error analysis for TSSP1 in 1D: errors at t=5.0 with $\Delta t = 0.0001$.

Δx	$\frac{1}{2}$	$\frac{1}{4}$	$\frac{1}{8}$
$\parallel \psi^e - \psi_{\Delta x, \Delta t} \parallel_2$	1.506e-02	2.715e-06	1.494e-11
$\parallel \phi^e - \phi_{\Delta x, \Delta t} \parallel_2$	1.648e-02	3.179e-06	1.668e-11

Table 4.4: Spatial error analysis for TSSP2 in 1D: errors at t=5.0 with $\Delta t = 0.0001$.

Δt	$\frac{1}{20}$	$\frac{1}{40}$	$\frac{1}{80}$
$\parallel \psi^e - \psi_{\triangle x, \triangle y, \Delta t} \parallel_2$	2.212e-02	1.05e-02	5.2e-03
$\parallel \phi^e - \phi_{\triangle x, \triangle y, \Delta t} \parallel_2$	1.38e-02	6.9e-03	3.4e-03

Table 4.5: Temporal error analysis for TSSP1 in 2D: errors at t=5.0 with $(\triangle x, \triangle y) = \left(\frac{1}{32}, \frac{1}{32}\right)$.

4.3.2 Accuracy tests in 2D

Similarly, to test the numerical accuracy in 2D, we compute numerical solutions with a very fine mesh $(\triangle x, \triangle y) = \left(\frac{1}{32}, \frac{1}{32}\right)$ and a very small time step $\Delta t = 0.0001$, which are also denoted as the 'exact' solutions, ψ^e, ϕ^e. In addition, for brevity, we denote $\psi_{\Delta \mathbf{x}, \Delta t}$, $\phi_{\Delta \mathbf{x}, \Delta t}$ as our numerical solutions with mesh size $(\triangle x, \triangle y) = (h_x, h_y)$ and time step Δt. We solve the problem in the box $[-30, 30] \times [-30, 30]$.

In the computation, we take the following parameters $V_1(x, y) = V_2(x, y) = \frac{x^2 + y^2}{2}$, $\delta_1 = 1$, $\delta_2 = 0$, $\Omega = 1$, $g = 1$, $v = 1$, $\kappa = 1$ and $\beta_{11} : \beta_{12} : \beta_{21} : \beta_{22} = \beta(1 : 0.94 : 0.94 : 0.97)$ with $\beta = 10$. The terminal time is at t=5. Without loss of generality, we also choose a Gaussian function in 2D and a complex number as initial values, which are

$$\psi(x, y, 0) = \phi(x, y, 0) = \frac{1}{\sqrt{2\pi}} e^{-\frac{x^2 + y^2}{2}}, \ C(0) = 1 + i. \tag{4.60}$$

For time accuracy tests, we fix a fine mesh size $(\triangle x, \triangle y) = (h_x, h_y) = \left(\frac{1}{32}, \frac{1}{32}\right)$. Table 4.5 and Table 4.6 show discretization errors in time for TSSP1 (4.58) and TSSP2 (4.59) in 2D, respectively. For spatial accuracy tests, we fix a very small time step $\Delta t = 0.0001$. Spatial discretization errors of TSSP1 and TSSP2 in 2D space are shown in Table 4.7 and Table 4.8, respectively.

Δt	$\frac{1}{20}$	$\frac{1}{40}$	$\frac{1}{80}$
$\parallel \psi^e - \psi_{(\triangle x, \triangle y, \Delta t)} \parallel_2$	1e-03	4.001e-04	1e-04
$\parallel \phi^e - \phi_{\triangle x, \triangle y, \Delta t} \parallel_2$	8.297e-04	2.312e-04	5.668e-05

Table 4.6: Temporal error analysis for TSSP2 in 2D: errors at t=5.0 with $(\triangle x, \triangle y) = \left(\frac{1}{32}, \frac{1}{32}\right)$.

$(\triangle x, \triangle y)$	$(\frac{1}{2}, \frac{1}{2})$	$(\frac{1}{4}, \frac{1}{4})$	$(\frac{1}{8}, \frac{1}{8})$
$\parallel \psi^e - \psi_{\triangle x, \triangle y, \Delta t} \parallel_2$	1.152e-03	1.553e-07	4.560e-012
$\parallel \phi^e - \phi_{\triangle x, \triangle y, \Delta t} \parallel_2$	7.878e-04	1.236e-08	1.085e-13

Table 4.7: Spatial error analysis for TSSP1 in 2D: errors at t=5.0 with $\Delta t = 0.0001$.

$(\triangle x, \triangle y)$	$(\frac{1}{2}, \frac{1}{2})$	$(\frac{1}{4}, \frac{1}{4})$	$(\frac{1}{8}, \frac{1}{8})$
$\parallel \psi^e - \psi_{\triangle x, \triangle y, \Delta t} \parallel_2$	1.145e-03	1.749e-08	5.010e-013
$\parallel \phi^e - \phi_{\triangle x, \triangle y, \Delta t} \parallel_2$	6.030e-04	9.493e-09	8.245e-14

Table 4.8: Spatial error analysis for TSSP2 in 2D: errors at t=5.0 with $\Delta t = 0.0001$.

From Tables 4.5-4.8, we can conclude for 2D that (i) Scheme TSSP1 (4.58) is of spectral accuracy in space and first order in time; (ii) Scheme TSSP2 (4.59) is of spectral accuracy in space and second order in time; (iii) Scheme TSSP1 (4.58) and Scheme TSSP2 (4.59) have similar spatial accuracy.

4.3.3   Conservation of dynamics properties

Our time-splitting schemes TSSP1 (or TSSP2) also keep quite well the conservation laws of the coupled equations, such as conservation of energy (i.e., $E = E(\psi, \phi, C)$) and the total mass of two condensates (i.e., $N(\psi) + N(\phi)$), which have been proved analytically in previous sections. The numerical results are shown in Figure 4.1(a) (for 1D) and Figure 4.1(b) (for 2D). Furthermore, from Figure 4.2(b), we find that time evolution of the total condensate width in 2D is periodic, which agrees with the predication shown in previous section 4.1.

In the one-dimensional computation (cf. Figure 4.1(a) and Figure 4.2(a)), we take the following parameters $V_1(x) = V_2(x) = \frac{x^2}{2}$, $\delta_1 = 1$, $\delta_2 = 0$, $\Omega = 1$, $g = 1$, $v = 1$, $\kappa = 0$ and $\beta_{11} : \beta_{12} : \beta_{21} : \beta_{22} = \beta(1 : 0.94 : 0.94 : 0.97)$ with $\beta = 10$.

In the two-dimensional computation (cf. Figure 4.1(b) and Figure 4.2(b)), we take the following parameters $V_1(x, y) = V_2(x, y) = \frac{x^2 + y^2}{2}$, $\delta_1 = 1$, $\delta_2 = 0$, $\Omega = 1$, $g = 1$, $v = 1$, $\kappa = 0$ and $\beta_{11} : \beta_{12} : \beta_{21} : \beta_{22} = \beta(1 : 0.94 : 0.94 : 0.97)$ with $\beta = 10$.

4.4   Numerical results

In this section, we investigate the one-dimensional and two-dimensional dynamics of coupling BEC in optical resonators through numerical simulations. We have shown
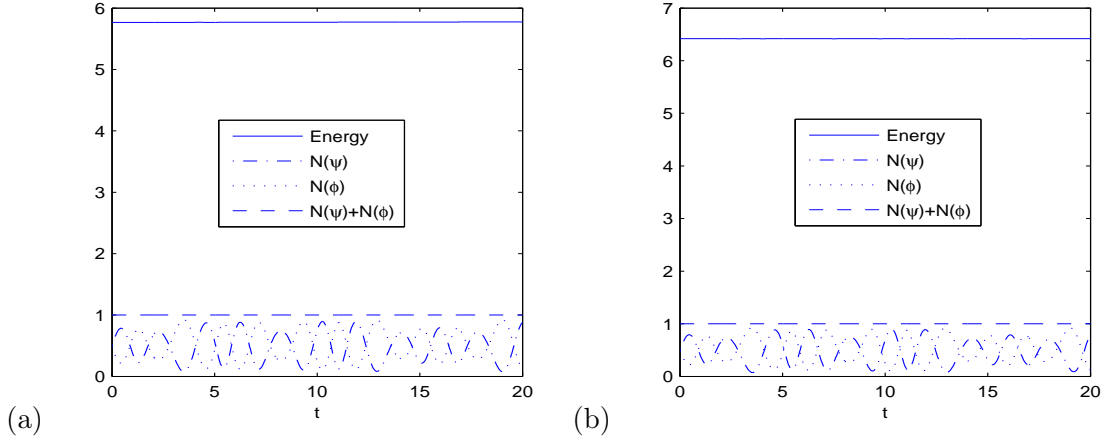
Figure 4.1: (a)Conservation of energy and the total mass of two condensates in 1D. (b)Conservation of energy and the total mass of two condensates in 2D.
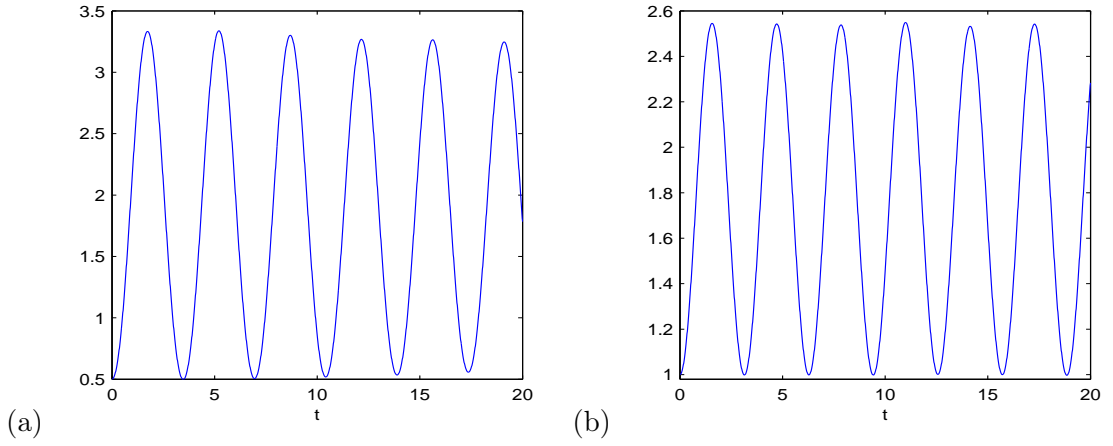

Figure 4.2: (a): Time evolution of the total condensate width in 1D. (b) time evolution of the total condensate width in 2D.

in the last section that the TSSP2 method (4.59) has spectral accuracy in space and second-order accuracy in time and it is better than the TSSP1 method (4.58). Therefore, in the computation presented below, we always take the TSSP2 method (4.59) in the simulations. The time step $\Delta t = 0.01$ and spatial mesh $\Delta x = \frac{1}{8}$ are applied in 1D. The time step $\Delta t = 0.01$ and spatial mesh $(\Delta x, \Delta y) = (\frac{1}{8}, \frac{1}{8})$ are used in 2D.

4.4.1 1D dynamical cases

In this subsection, we numerically study the one-dimensional dynamics of coupling BEC in optical resonators. In the computation, we choose parameters as $V(x) = \frac{x^2}{2}$, $\delta_1 = 1$, $\delta_2 = 0$, $\Omega = 1$, $g = 1$, $v = 1$, and $\beta_{11} : \beta_{12} : \beta_{21} : \beta_{22} = \beta(1 : 0.94 : 0.94 :$

0.97) with $\beta = 10$. We choose the computation interval $[a, b]$ as $[-30, 30]$. We prepare the initial data for the dynamics with the ground state solutions, which are obtained through the method introduced in Chapter 3.

After the preparation of ground state solutions as initial data, we investigate the dynamics of ground state solutions by solving the coupled equations (4.20)-(4.22) in 1D while suddenly changing the physically-related parameters (such as the coupling strength g, the detuning strength δ_1, or the effective Rabi frequency Ω) at time t=0.
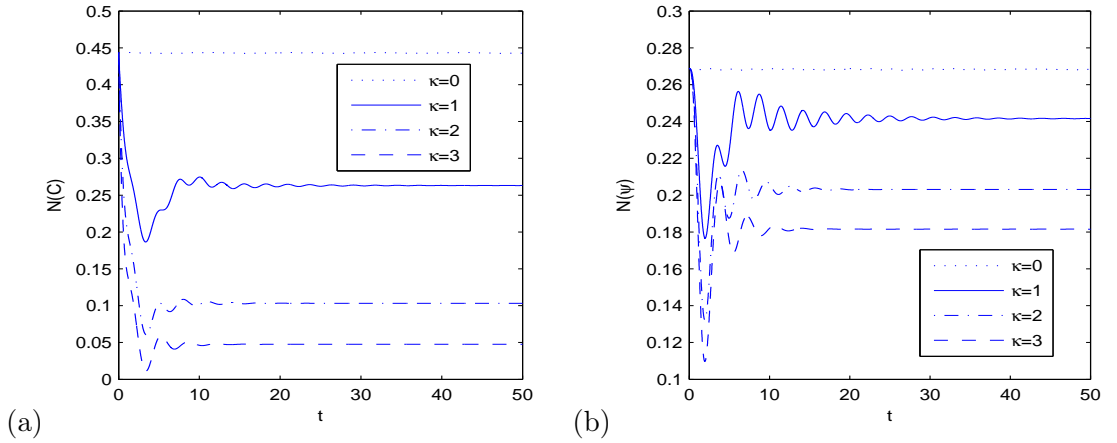
Figure 4.3: (a) time evolution of photons mass N(C) for different κ; (b) time evolution of mass of ψ for different κ

.

Figure 4.3 shows the dynamics of mass of photons $N(C)$ and mass of one condensate $N(\psi)$ respectively, when different κ are applied at time $t = 0$. Since the total mass of the two condensates, i.e. $N(\psi) + N(\phi)$, is equal to 1 for any κ, we only plot for $N(\psi)$ here. We can see from Figure 4.3 that (i) both $N(C)$ and $N(\psi)$ decay to a stable value as $t \to \infty$ when $\kappa \neq 0$; (ii) both $N(C)$ and $N(\psi)$ are conserved as $t \to \infty$ when $\kappa = 0$.

As our motivation is to study on how to unite two condensates into a bigger one by putting the coupling BEC in a dissipative ring cavity, we do the numerical simulation with $\kappa = 1$ for illustration purpose.

Figure 4.4 shows us the dynamics of mass of two condensates, i.e., $N(\psi)$ and $N(\phi)$ when different g are applied at time $t = 0$. Furthermore, from Figure 4.5, we can find that $N(\psi) \to 1$ and $N(\phi) \to 0$ as larger g are applied.

Figure 4.6 shows us the dynamics of mass of two condensates, i.e., $N(\psi)$ and $N(\phi)$ when different δ_1 are applied at time $t = 0$. From Figure 4.7, we can find that $N(\psi) \to 1$
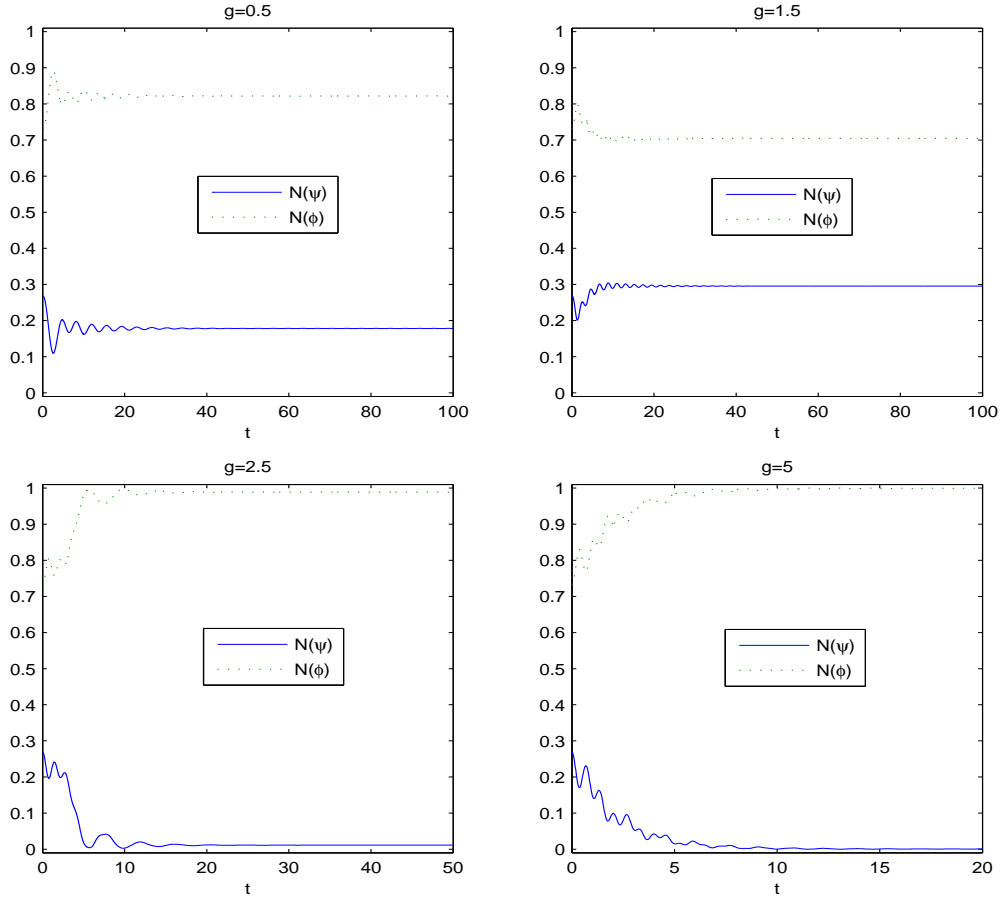
Figure 4.4: Time evolution of mass of two condensates when different g are applied at time $t = 0$.

and $N(\phi) \to 0$ as larger δ_1 are applied.

Figure 4.8 shows dynamics of mass of two condensates, i.e., $N(\psi)$ and $N(\phi)$ when different Ω are applied at time $t = 0$. Furthermore, from Figure 4.9, we may deduce that $N(\psi) \to N(\phi)$ as Ω gets larger.

When the system is put in a dissipative ring cavity ($\kappa = 1$), from the long-time simulations shown in Figures 4.4-4.7, we can observe that the sudden change of coupling strength g or detuning strength δ_1 at $t = 0$ may form a bigger BEC at large time t by transferring one into the other, which we interpret as a kind of 'fusion' sense since two independent BEC become a unique one. From the simulations shown in Figures 4.8-4.9, we conclude that the sudden change of effective Rabi frequency Ω at $t = 0$ may unite the coupling BEC into a bigger one, which we also interpret as another kind of 'fusion' by some senses observed via mass or density plots. We will then show density plots in
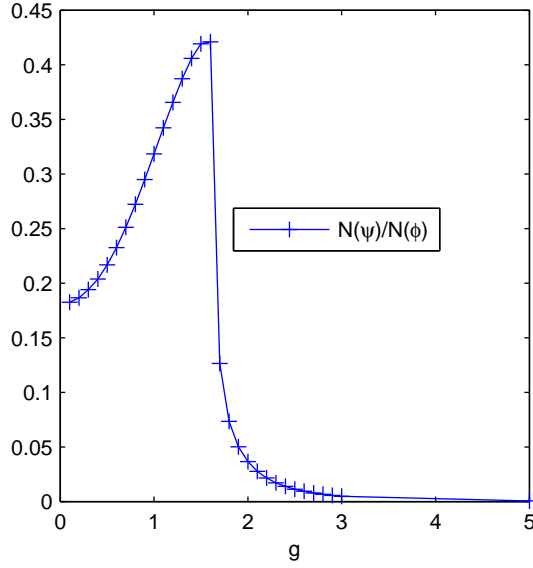
Figure 4.5: Ratio $\frac{N(\psi)}{N(\phi)}$ against g after $t = 100$.

2D cases.

4.4.2 2D Dynamical cases

In this subsection, we numerically study the two-dimensional dynamics of coupling BEC in optical resonators. We compute a ground state as initial data. Here, We choose domain $[-30, 30] \times [-30, 30]$, and mesh size $h_x = h_y = 1/8$. We set parameters $g = 1$ $\Omega = 1$, $\delta_1 = 1, \delta_2 = 0$, $V_1(x, y) = V_2(x, y) = \frac{1}{2}(x^2 + y^2)$ and $[\beta_{11} : \beta_{12} : \beta_{21} : \beta_{22}] = 100 \times (1 : 0.94 : 0.94 : 0.97)$.

We prepare the initial data for studying the dynamics with the ground state solutions, which are obtained through the method introduced in Chapter 3. In computing the ground state solutions, we choose above-mentioned parameters. Figure 4.10 shows us the density plots for the initial data in 2D.

After the initial data are obtained, we investigate the dynamics of ground state solutions by solving the coupled equations (4.20)-(4.22) in 2D while suddenly changing the physically-related parameters (such as the coupling strength g, the detuning strength δ_1, or the effective Rabi frequency Ω) at time t=0. Again, we keep the decay rate $\kappa = 1$ in the simulations for the same reason as those in 1D.

Figure 4.11 shows us the dynamics of mass of two condensates, i.e., $N(\psi)$ and $N(\phi)$
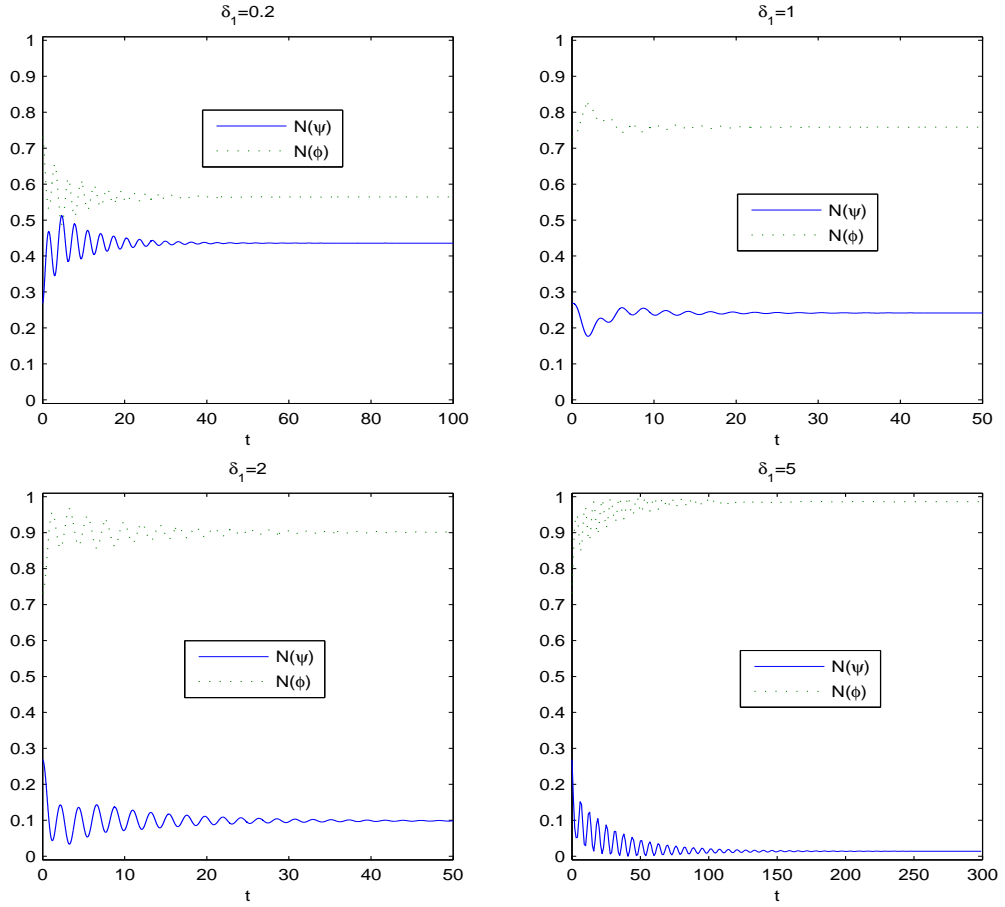
Figure 4.6: Time evolution of mass of two condensates when different δ_1 are applied at time $t = 0$.

when $g = 0.5$ and $g = 5$ are applied at time $t = 0$ respectively. From this Figure , we can find that $N(\psi) \to 1$ and $N(\phi) \to 0$ as the larger $g = 5$ is applied. The density plots for the wave-functions at $t = 30$ are shown in Figure 4.12, which further illustrates our observations.

Figure 4.13 shows us the dynamics of mass of two condensates, i.e., $N(\psi)$ and $N(\phi)$ when $\delta_1 = 0.5$ and $\delta_1 = 2$ are applied at time $t = 0$ respectively. From this Figure , we can observe that $N(\psi) \to 1$ and $N(\phi) \to 0$ as the larger $\delta_1 = 2$ is applied. The density plots for the wave-functions at $t = 50$ are shown in Figure 4.14, which further illustrates our observations.

Figure 4.15 shows us the dynamics of mass of two condensates, i.e., $N(\psi)$ and $N(\phi)$ when $\Omega = 0.1$ and $\Omega = 2$ are applied at time $t = 0$ respectively. From this Figure, we can observe that $N(\psi) \to N(\phi)$ as the larger $\Omega = 2$ is applied. The density plots for
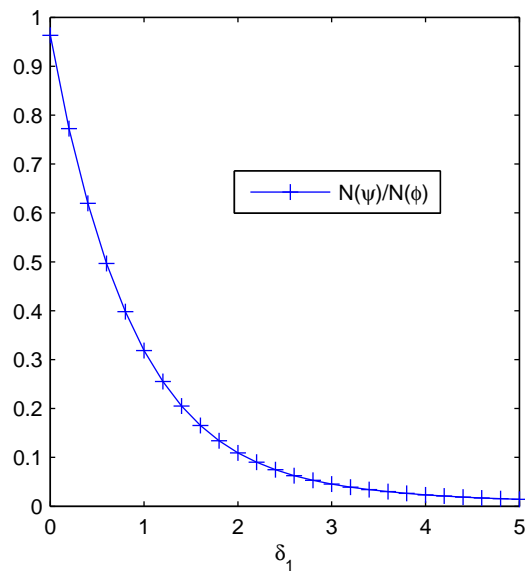
Figure 4.7: Ratio $\frac{N(\psi)}{N(\phi)}$ against δ_1 after $t = 200$.

the wave-functions at $t = 200$ are shown in Figure 4.16, which further illustrates our observations.

When the system are put in a dissipitative ring cavity ($\kappa = 1$), from our two-dimensional simulations shown in Figures 4.11-4.16, we can predict that a 'fusion' sense may occur with the sudden change of coupling strength g, detuning strength δ_1 or effective Rabi frequency Ω at $t = 0$, which also agrees with our one-dimensional simulations in section 4.4.1.
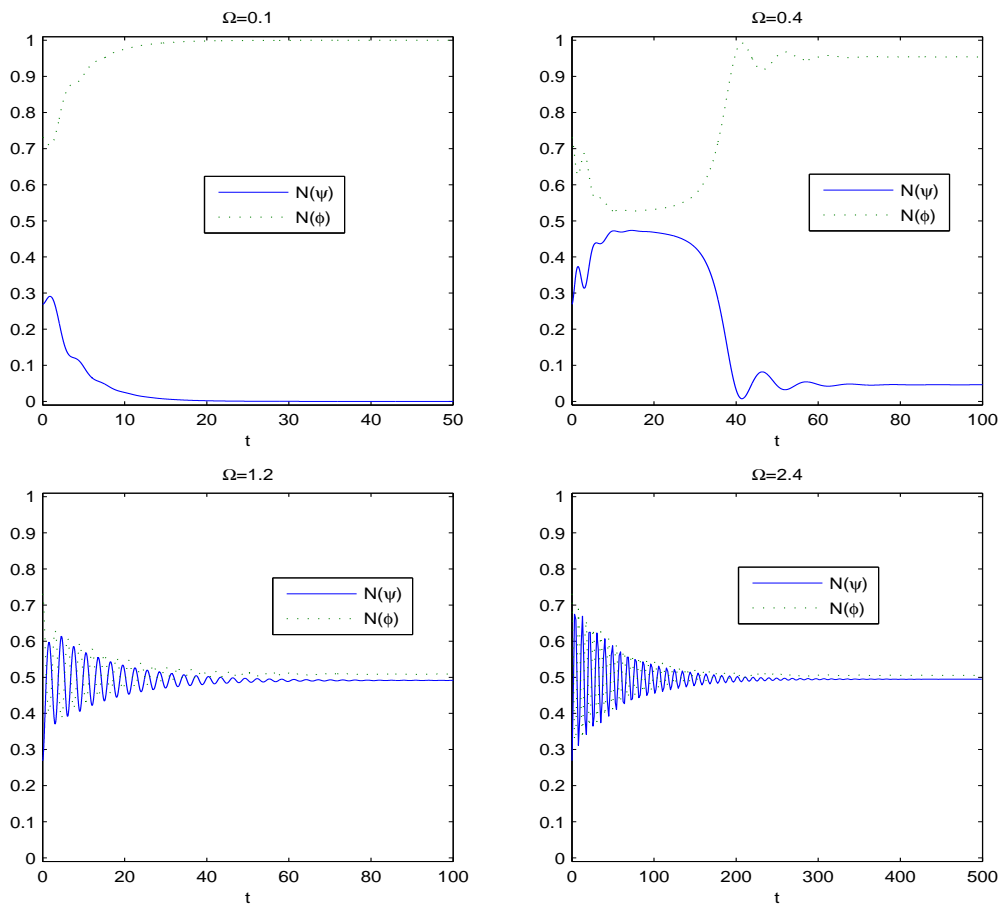
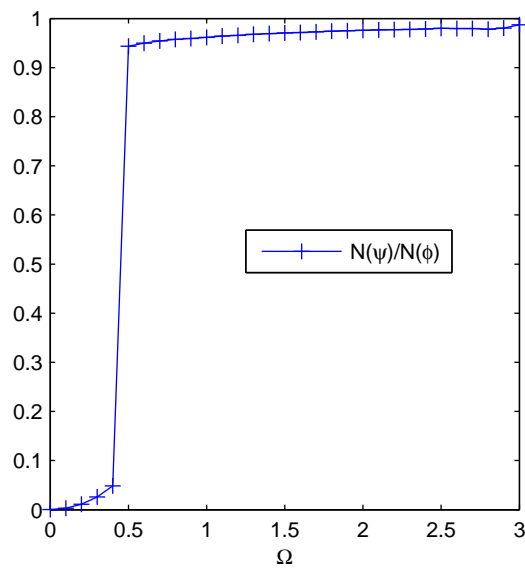Figure 4.8: Time evolution of mass of two condensates when different Ω are applied at time $t = 0$.

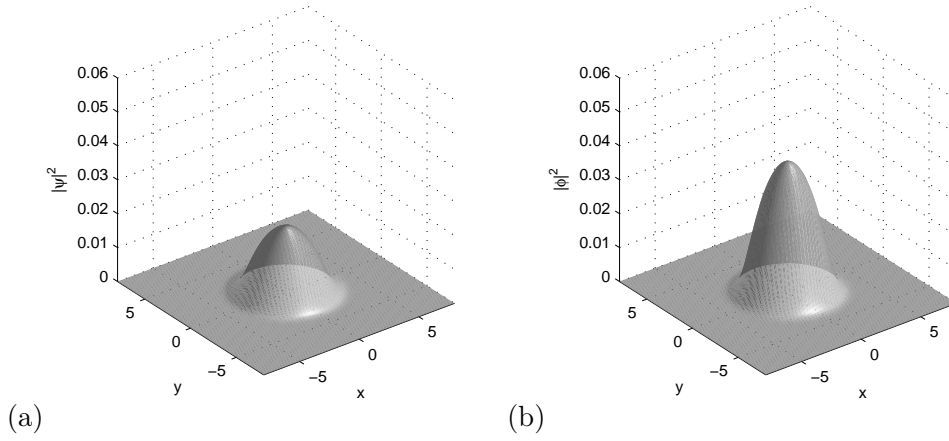Figure 4.9: Ratio $\frac{N(\psi)}{N(\phi)}$ against Ω after $t = 100$.

(a)   (b)

Figure 4.10: Density plots of the ground states solutions, which are used as initial data for studying the dynamics in 2D.
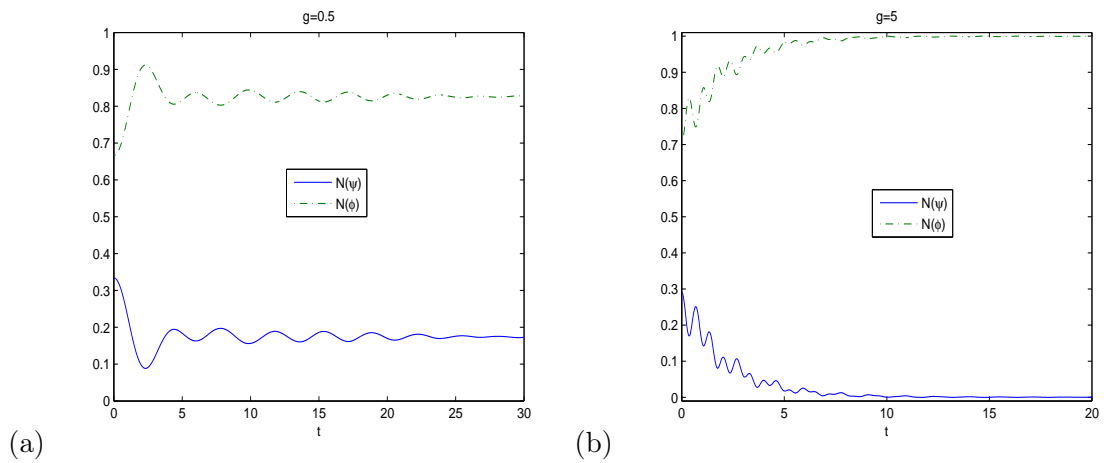

(a)   (b)

Figure 4.11: (a) Time evolution of mass of two condensates: (a) $g = 0.5$; (b) $g = 5$.
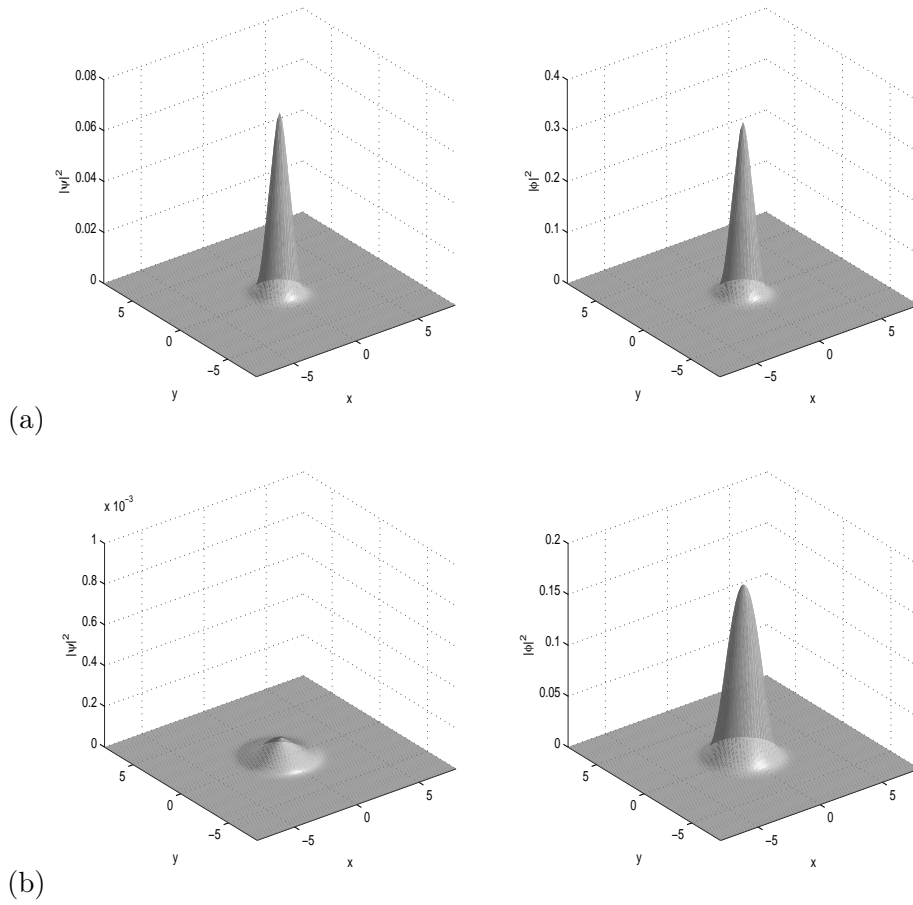
Figure 4.12: Density plots for the wave-functions at $t = 30$: (a) $g = 0.5$; (b)$g = 5$.

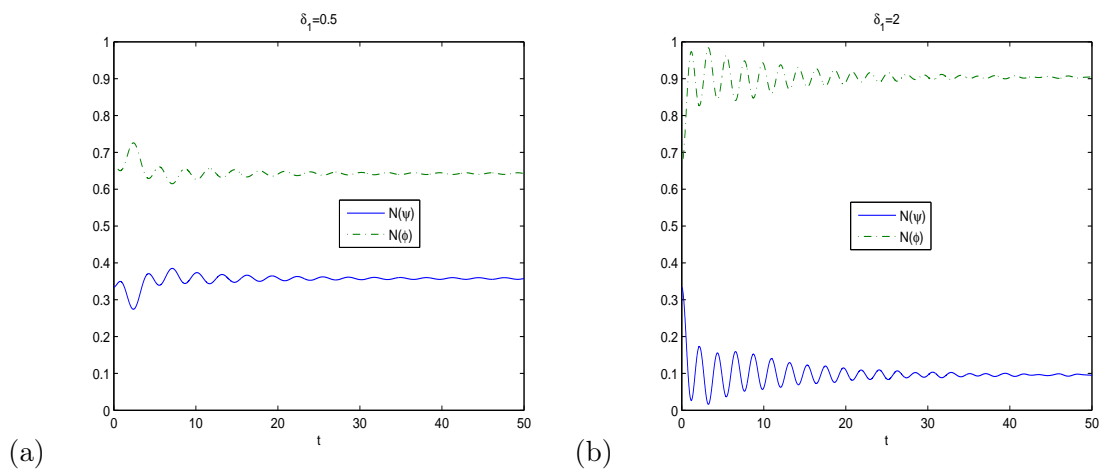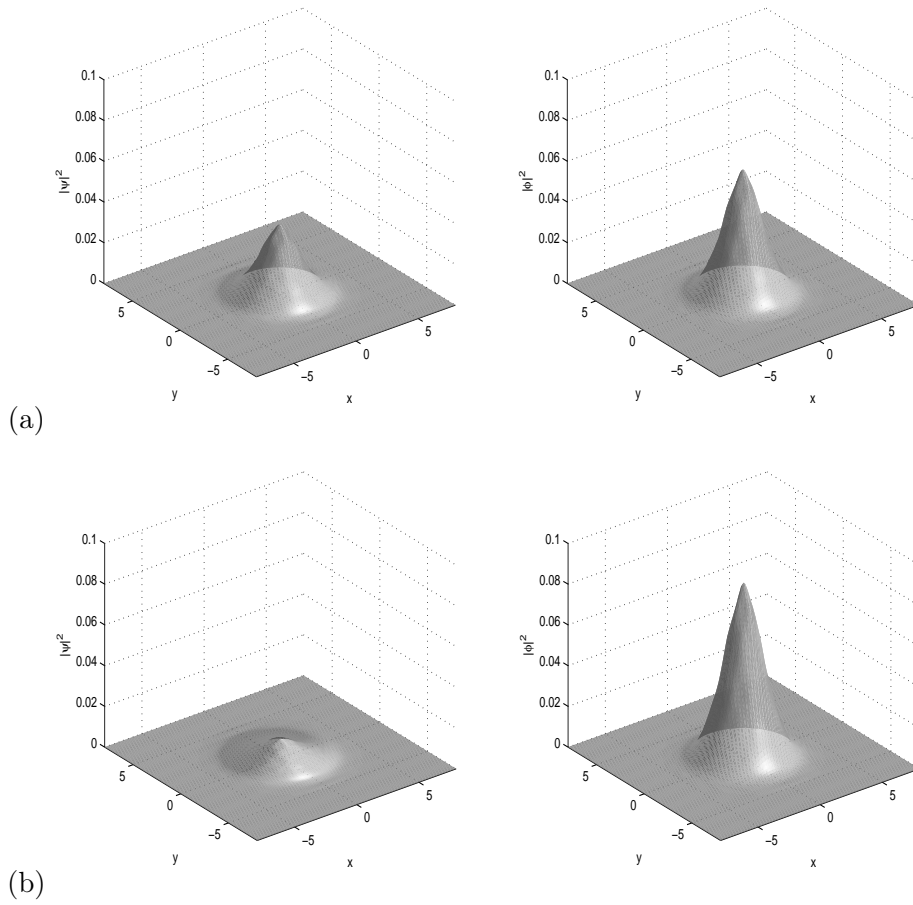Figure 4.13: Time evolution of mass of two condensates: (a) $\delta_1 = 0.5$; (b) $\delta_1 = 2$.

Figure 4.14: Density plots for the wave-functions at $t = 50$: (a) $\delta_1 = 0.5$; (b) $\delta_1 = 2$.
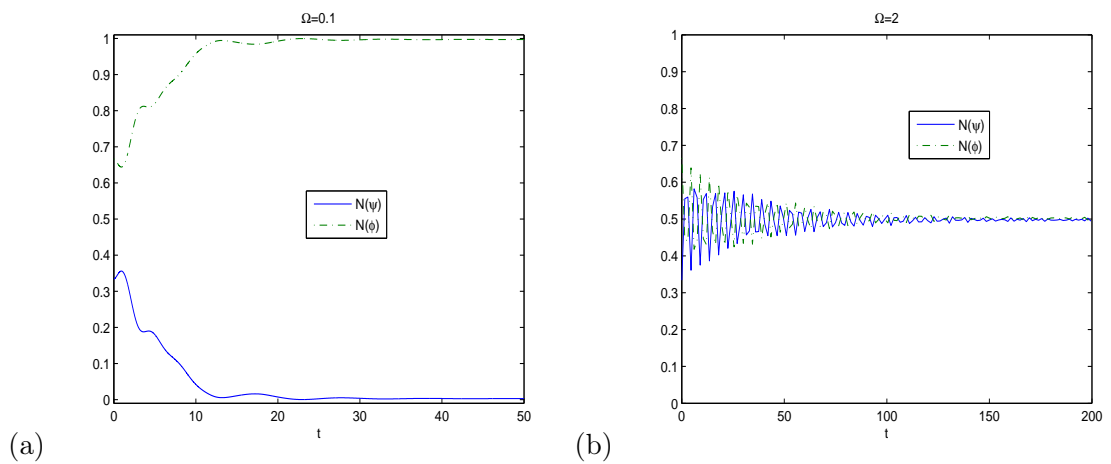

Figure 4.15: Time evolution of mass of two condensates: (a) $\Omega = 0.1$; (b) $\Omega = 2$.

(a)

(b)
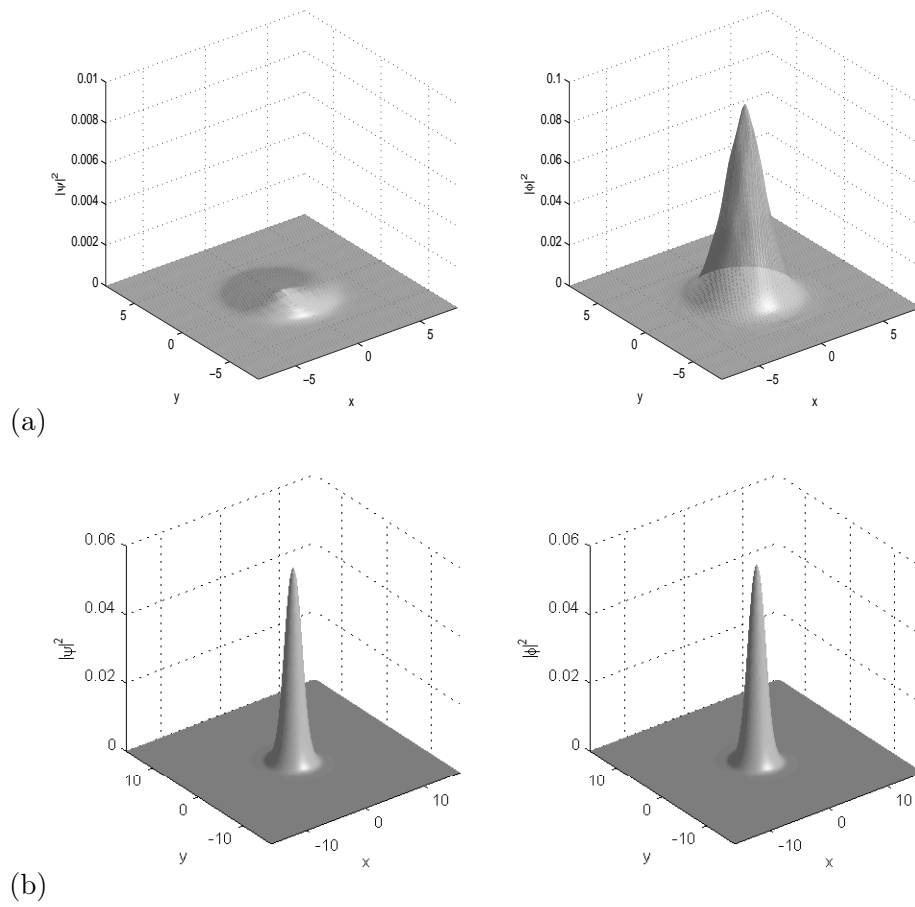
Figure 4.16: Density plots for the wave-functions at $t = 200$: (a) $\Omega = 0.1$; (b) $\Omega = 2$.

Chapter 5

Conclusion

We have analytically and numerically studied ground states and dynamics of coupling BEC in optical resonators by solving the mathematical model— Gross-Pitaevskii equations coupled with an integral and ordinary differential equation.

In the analysis and computation of ground state solutions, we have proposed that the continuous gradient flow will propagate to the ground state if proper initial data are chosen. To simplify the discretization of the continuous gradient flows, we have designed a gradient flow with discrete normalization, which is an efficient way to find the ground states as proved in our intensive numerical tests. By discretizing the normalized gradient flow with the backward Euler Sine pseudospectral method, we numerically have found various ground state structures of coupling BEC in optical resonators, both in 1D and 2D. We found that ground state solutions' structure depends on many factors, such as types of trapping potential which have been applied, the particle number of the condensates, the coupling strength, the Rabi frequency and so on. We noticed that the density of two condensates become closer and closer as the coupling strength g grows larger, though the condensates are confined in different trapping potentials. This observation may suggest that cavity strength g promote the union of two condensates when they are in ground states.

In the analysis and computation of dynamics, we have proved some conservation laws related to the coupled equations which model the dynamics of coupling BEC in optical resonators, for example the conservation of the total mass and the conservation of the energy. We also investigated dynamical property of condensate width and we

found that it is periodic with respect to time t under some assumptions. We presented two time-splitting Sine pseudospectral methods (TSSP1 and TSSP2) for computing the dynamics. We have observed that both methods have spectral accuracy in space and both methods keep the conservation laws quite well. Furthermore we noticed from long time simulations that a 'fusion' sense may occur with the sudden change of coupling strength g, detuning strength δ_1 or effective Rabi frequency Ω.

In future, we plan to do three-dimensional simulations for the ground states and dynamics of coupling BEC in optical resonators. We believe the proposed efficient numerical methods and their applications can predict more physically interesting phenomena.

Bibliography

[1] A. Aftalion, I. Danaila, Three-dimensional vortex configurations in a rotating Bose-Einstein condensate, Phys. Rev. A, 68 (2003), article 023603.

[2] S. K. Adhikari, P. Muruganandam, Bose-Einstein condensation dynamics from the numerical solution of the Gross-Pitaevskii equation, J. Phys. B: At. Mol. Opt. Phys., 35 (2002), pp. 2831-2843.

[3] S. N. Bose, Plancks Gesetz und Lichtquantenhypothese, *ZeitschiftFürPhysik* A, 26 (1924), pp. 178-181.

[4] W. Bao, Ground states and dynamics of multi-component Bose-Einstein condensates, SIAM Multiscale Modeling and Simulation, 2 (2004), pp. 210-236.

[5] W. Bao, Q. Du, Computing the ground state solution of Bose-Einstein condensates by a normalized gradient flow, SIAM J. Sci. Comput., 25 (2004), pp. 1674-1697.

[6] W. Bao, D. Jaksch, and P.A. Markowich, Numerical solution of the Gross-Pitaevskii equation for Bose-Einstein condensation, J. Comput. Phys., 187 (2003), pp. 318-342.

[7] W. Bao, J. Shen, A Fourth-order time-splitting Laguerre-Hermite pseudospectral method for Bose-Einstein condensates, SIAM J. Sci. Comput., 26 (2005), pp. 2010-2028.

[8] W. Bao, Shi Jin, and P.A. Markowich, On time-splitting spectral approximations for the Schrödinger equation in the semiclassical regime, J. Comput. Phys., 175 (2002), pp. 487 - 524.

[9] W. Bao, W. Tang, Ground-state solution of Bose-Einstein condensate by directly minimizing the energy function, J.Comp. Phys., 187 (2003), pp. 230-254.

[10] W. Bao, H. Wang, and P.A. Markowich, Ground, symmetric and central vortex states in rotating Bose-Einstein condensates, Comm. Math. Sci., 3 (2005), pp. 57-88.

[11] W. Bao, Y. Zhang, Dynamics of the ground state and central vortex states in Bose-Einstein condensation, Math. Mod. Meth. Appl. Sci., 15 (2005), pp. 1863-1896.

[12] W. Bao, Y. Zhang, Dynamical laws of the coupled Gross-Pitaevskii equations for spin-1 Bose-Einstein condensates, Meth. Appl. Anal., to appear.

[13] W. Bao, Y. Zhang, and H. Li, Dynamics of rotating two-component Bose-Einstein condensates and its efficient computation, Physica D, 234 (2007), pp. 49-69.

[14] R. A. Battye, N. R. Cooper, and P. M. Sutcliffe, Stable skyrmions in two-Component Bose-Einstein condensates, Phys. Rev. lett., 88 (2002), article 080401.

[15] B. M. Caradoc-Davis, R. J. Ballagh, and P. B. Blakie, Three-dimensional vortex dynamics in Bose-Einstein condensates, Phys. Rev. A, 62 (2000), article 011602.

[16] B. M. Caradoc-Davis, R. J. Ballagh, and P. B. Blakie, Coherent dynamics of vortex formation in trapped Bose-Einstein condensates, Phys. Rev. Lett., 83 (1999), pp. 895-898.

[17] M. M. Cerimele, M. L. Chiofalo, F. Pistella, S. Succi, and M. P. Tosi, Numerical solution of the Gross-Pitaevskii equation using an explicit finite difference scheme: an application to trapped Bose-Einstein condensates, Phys. Rev. E, 62 (2000), pp. 1382-1389.

[18] K. Doi, Y. Natsume, Simulations of dynamics for wavepackets made by two-component Bose-Einstein condensates in Alkali-atom gases, Physica B, 329 (2003), pp. 49-50.

[19] F. Dalfovo, S. Stringari, Bosons in anisotropic traps: Ground state and vortices, Phys. Rev. A, 53 (1996), pp. 2477-2485.

[20] A. Einstein, Quantentheorie des einatomigen idealen gases, Sitzber. Kgl. Preuss. Akad. Wiss., 142 (1924), pp. 261-267.

[21] M. Edwards, K. Burnett, Numerical solution of the nonlinear Schrödinger equation for small samples of trapped neutral atoms, Phys. Rev. A, 51 (1995), pp. 1382-1386.

[22] M. Edwards, R. J. Dodd, C. W. Clark, P. A. Ruprecht, and K. Burnett, Properties of a Bose-Einstein condensate in an anisotropic harmonic potential, Phys. Rev. A, 53 (1996), pp. R1950-R1953.

[23] E. P. Gross, Structure of a quantized vortex in boson systems, Nuovo. Cimento., 20 (1961), pp. 454-477.

[24] D. S. Hall, M. R. Matthews, J. R. Ensher, C. E. Wieman, and E. A. Cornell, Dynamics of component separation in a binary mixture of Bose-Einstein condensates, Phys. Rev. Lett., 81 (1998), pp. 1539-1542.

[25] D. S. Hall, M. R. Mattews, C. E. Wieman, and E. A. Cornell, Measurements of relative phase in two-component Bose-Einstein condensates, Phys. Rev. Lett., 81 (1998), pp. 1543-1546.

[26] T. L. Ho, V. B. Shenoy, Binary mixtures of Bose Condensates of Alkali atoms, Phys. Rev. Lett., 77 (1996), pp. 3276-3279.

[27] D. Jaksch, S.A. Gardiner, K. Schulze, J.I. Cirac, and P. Zoller, Uniting Bose-Einstein condensates in optical resonators, Phys. Rev. Lett., 86 (2001), pp. 4733-4736.

[28] B. Jackson, J. F. McCann, and C. S. Adams, Vortex formation in dilute inhomogeneous Bose-Einstein condensates, Phys. Rev. Lett., 80 (1998), pp. 3903-3906.

[29] B. Jackson, J. F. McCann, and C. S. Adams, Vortex line and ring dynamics in trapped Bose-Einstein condensates, Phys. Rev., A 61 (1999), 013604.

[30] C. Y. Lin, E. J. V. de Passos, and D. S. Lee, Time-dependent variational analysis of Josephson oscillations in a two-component Bose-Einstein condensate, Phys. Rev. A, 62 (2000), article 055603.

[31] E. H. Lieb, J. P. Solovej, Ground state energy of the two-component charged Bose gas, Comm. Math. Phys., 252 (2004), pp. 485-534.

[32] T. -C. Lin, J. Wei, Spikes in two-component systems of nonlinear *Schröinger* equations with trapping potentials, J. Diff. Equ., 229 (2006), pp. 538-569.

[33] E. Lundh, C.J. Pethick, and H. Smith, Vortices in Bose-Einstein condensated atomic clouds, Phys. Rev. A, 58 (1998), pp. 4816-4823.

[34] K. W. Madison, F. Chevy, W. Wohlleben, and J. Dal- ibard, Vortex formation in a stirred Bose-Einstein condensate, Phys. Rev. Lett., 84 (2000), pp. 806-809.

[35] M. R. Matthews, B. P. Anderson, P. C. Haljan, D. S. Hall, C. E. Wieman, and E. A. Cornell, Vortices in a Bose-Einstein condensate, Phys. Rev. Lett., 83 (1999), pp. 2498-2501.

[36] P. Muruganandam, S. K. Adhikari, Bose-Einstein dynamics in three dimensions by the pseudospectral and finite-difference methods, J. Phys. B: At. Mol. Opt. Phys., 36 (2003), pp. 2501-2513.

[37] Myatt, E. A. Burt, R. W. Ghrist, E. A. Cornell, and C. E. Wieman, Production of two overlapping Bose-Einstein condensates by sympathetic cooling, Phys. Rev. Lett., 78 (1997), pp. 586-589.

[38] M. Modugno, F. Dalfovo, C. Fort, P. Maddaloni, and F. Minardi, Dynamics of two colliding Bose-Einstein condensates in an elongated magnetostatic trap, Phy. Rev. A, 62 (2000), article 063607.

[39] M. Modugno, L. Pricoupenko, and Y. Castin, Bose-Einstein condensates with a bent vortex in rotating traps, Eur. Phys. J. D, 22 (2003), pp. 235-257.

[40] E. J. Mueller, T.-L. Ho, Two-component Bose-Einstein condensates with a large number of vortices, Phys. Rev. Lett., 88 (2002), article 180403.

[41] J. C. Neu, Vortices in complex scalar fields, Physica D, 43 (1990), pp. 385-406.

[42] J. C. Neu, Vortex dynamics of the nonlinear wave equation, Physica D, 43 (1990), pp. 407-420.

[43] Y. N. Ovchinnikov, I. M. Sigal, The Ginzburg-landau equation I. Static vortices, Part. Diff. Eqn and their Appl. CRM proceedings, 12 (1997), pp. 199-220.

[44] Y. N. Ovchinnikov, I. M. Sigal, The Ginzburg-Landau equation III. vortex dynamics, Nonlinearity, 11 (1998), pp. 1277-1294.

[45] Y. N. Ovchinnikov, I. M. Sigal, Long-time behaviour of Ginzburg-Landau vortices, Nonlinearity, 11 (1998), pp. 1295-1309.

[46] L. P. Pitaevskii, Vortex lines in a imperfect Bose gase, Zh. Eksp. Teor. Fiz., 40 (1961), pp. 646-649.

[47] L. P. Pitaevskii, S. Stringari, Bose-Einstein condensation, Clarendon Press, New York, (2003).

[48] C. Raman, J. R. Abo-Shaeer, J. M. Vogels, K. Xu, and W. Ketterle, Vortex nucleation in a stirred Bose-Einstein condensate, Phys. Rev. Lett., 87 (2001), article 210402.

[49] P. Rosenbuch, V. Bretin, and J. Dalibard, Phys. Rev. lett., 89 (2002), article 200403.

[50] P. A. Ruprecht, M. J. Holland, K. Burnett, and M. Edwards, Time-dependent solution of the nonlinear Schrodinger equation for Bose-condensed trapped neutral atoms, Phys. Rev. A, 51 (1995), pp. 4704-4711.

[51] F. Riboli, M. Modugno, Topology of the ground state of two interacting Bose-Einstein condensates, Phys. Rev. A, 65 (2002), article 063614.

[52] D. M. Stamper-kurn, M. R. Andrews, A. P. Chikkatur, S. Inouye, H.-J. Miesner, J. Stenge, and W. Ketterle, Optical confinement of a Bose-Einstein condensate, Phys. Rev. Lett., 80 (1998), pp. 2027-2030.

[53] B. I. Schneider, D.L. Feder, Numerical approach to the ground and excited states of a Bose-Einstein condensated gas confined in a completely anisotropic trap, Phys. Rev. A, 59 (1999), pp. 2232-2242.

[54] A. Sinatra, P. O. Fedichev, Y. Castin, J. Dalibard, and G. V. Shlyapnikov, Dynamics of two interacting Bose-Einstein condensates, Phys. Rev. Lett., 82 (1999), pp. 251-254.

[55] A. A. Svidzinsky, A. L. Fetter, Dynamics of a vortex in a trapped Bose-Einstein condensate, Phys. Rev., A 62 (2000), article 063617.

[56] G. L. Salmond, C. A. Holmes, and G. J. Milburn, Dynamics of a strongly driven two-component Bose-Einstein condensate, Phys. Rev. A, 65 (2002), article 033623.

[57] M. Tsubota, K. Kasamatsu, and T. Araki, Dynamics of quantized vortices in superfluid helium and rotating Bose-Einstein condensates, cond-mat/0309364.

[58] M. Trippenbach, K. Góral, K. Rzążewski, B. Malomed, and B Band, Structure of binary Bose-Einstein condensates, J. Phys. B: At. Mol. Opt. Phys., 33 (2000), pp. 4017-4031.

[59] V. Vekslerchik, V. M. Pérez-García, Exact solution of the two-mode model of multicomponent Bose-Einstein condensates, Discrete and Continuous Dynamical Systems B, 3 (2003), pp. 179-192.

[60] H. Wang, Numerical studies on the split step finite differnce method for nonlinear Schrödinger equations, Appl. Math. Comput., 170 (2005), pp. 17-35.

[61] H. Wang, A time-splitting spectral method for computing dynamics of spinor F=1 Bose-Einstein condensates, Int. J. Comput. Math., 84 (2007), pp. 925-944.

[62] H. Wang, Numerical simulations on stationary states for rotating two-component Bose-Einstein condensates, J. Sci. Ccmput., 38 (2009), pp. 149-163.

[63] H. Wang, Quantized Vortex states and dynamics in Bose-Einstein condensates, PhD thesis, National University of Singapore, (2006).

[64] H. Wang, W. Xu, An efficient numerical method for simulating the dynamics of coupling Bose-Einstein condensates in optical resonators, Computer Physics Communications, 182 (2011), pp. 706-718.

[65] J. E. Williams, M. J. Holland, preparing topological states of a Bose-Einstein condenstate, Nature, 401 (1999), pp. 568-571.

[66] W. Zhang, S. Yi, and L. You, Mean field ground state of a spin-1 condensate in a magnetic field, New J. Phys., 5 (2003), pp. 77.1-77.12.

[67] Y. Zhang, Mathematical analysis and numerical simulation of Bose-Einstein condensation, PhD thesis, National University of Singapore, (2006).

Name: Xu Wei Biao

Degree: Master

Department: Mathematics

Thesis Title: Analysis and Computation for Coupling Bose-Einstein Condensates in Optical Resonators

Abstract

In this thesis, we unveil some properties of a mathematical model for coupling two-component Bose-Einstein condensate in the optical resonators. We propose a normalized gradient flow method with backward Euler Sine pseudospectral approach to compute the ground state. We also use our numerical solutions to study which factors may be useful for uniting BEC in optical resonators at equilibrium. By adjusting time-splitting Sine spectral methods to solve the model, we investigate the dynamics via simulating the dissipative process and interpret a 'fusion' sense through observations from the results.

Keywords Coupling Bose-Einstein condensate, optical resonators, gradient flow with discrete normalization, time-splitting Sine spectral methods.